



1 **Frozen-soil hydrological modeling for a mountainous catchment**
2 **at northeast of the Tibetan Plateau**

3

4 Hongkai Gao 1, 2*, Chuntan Han 3, Rensheng Chen 3, Zijing Feng 2, Kang Wang 1,2,
5 Fabrizio Fenicia 4, Hubert Savenije 5

6

7 1 Key Laboratory of Geographic Information Science (Ministry of Education of China), East
8 China Normal University, Shanghai, China

9 2 School of Geographical Sciences, East China Normal University, Shanghai, China

10 3 Qilian Alpine Ecology and Hydrology Research Station, Key Lab. of Ecohydrology of Inland
11 River Basin, Northwest Institute of Eco-Environment and Resources, Chinese Academy of
12 Sciences, Lanzhou 730000, China

13 4 Eawag, Swiss Federal Institute of Aquatic Science and Technology, Dübendorf, Switzerland

14 5 Delft University of Technology, Delft, the Netherlands

15 *Corresponding to: Hongkai Gao (hkgao@geo.ecnu.edu.cn)

16

17 **Abstract:**

18 Increased attention directed at frozen-soil hydrology has been prompted by climate
19 change. In spite of an increasing number of field measurements and modeling studies, the
20 impact of frozen-soil on hydrological processes at the catchment scale is still unclear.
21 However, frozen-soil hydrology models have mostly been developed based on a "bottom-
22 up" approach, i.e. by aggregating prior knowledge at pixel scale, which is an approach
23 notoriously suffering from equifinality and data scarcity. Therefore, in this study, we explore
24 the impact of frozen-soil at catchment-scale, following a "top-down" approach, implying:
25 expert-driven data analysis → qualitative perceptual model → quantitative conceptual
26 model → testing of model realism. The complex mountainous Hulu catchment, northeast of
27 the Tibetan Plateau, was selected as the study site. Firstly, we diagnosed the impact of
28 frozen-soil on catchment hydrology, based on multi-source field observations, model
29 discrepancy, and our expert knowledge. Two new typical hydrograph properties were
30 identified: the low runoff in the early thawing season (LRET) and the discontinuous baseflow
31 recession (DBR). Secondly, we developed a perceptual frozen-soil hydrological model, to
32 explain the LRET and DBR properties. Thirdly, based on the perceptual model and a
33 landscape-based modeling framework (FLEX-Topo), a semi-distributed conceptual frozen-
34 soil hydrological model (FLEX-Topo-FS) was developed. The results demonstrate that the
35 FLEX-Topo-FS model can represent the effect of soil freeze/thaw processes on hydrologic



36 connectivity and groundwater discharge and significantly improve hydrograph simulation,
37 including the LRET and DBR events. Furthermore, its realism was confirmed by alternative
38 multi-source and multi-scale observations, particularly the freezing and thawing front in the
39 soil, the lower limit of permafrost, and the trends in groundwater level variation. To the best
40 of our knowledge, this study is the first report of LRET and DBR processes in a mountainous
41 frozen-soil catchment. The FLEX-Topo-FS model is a novel conceptual frozen-soil
42 hydrological model, which represents these complex processes and has potential for wider
43 use in the vast Tibetan Plateau and other cold mountainous regions.

44

45 1 Introduction

46 1.1 Frozen-soil hydrology: one of twenty-three unsolved problems

47 The Tibetan Plateau is largely covered by frozen soil and is characterized by a fragile cold
48 and arid ecosystem (Immerzeel et al., 2010; Ding et al., 2020). As this region serves as the
49 “water tower” for nearly 1.4 billion people, understanding the frozen soil hydrology is
50 important for regional and downstream water resources management and ecosystem
51 conservation. Frozen soil prevents vertical water flow which often leads to saturated soil
52 conditions in continuous permafrost, while confining subsurface flow through perennially
53 unfrozen zones in discontinuous permafrost (Walvoord and Kurylyk, 2016). As an aquiclude
54 layer, frozen soil substantially controls surface runoff and its hydraulic connection with
55 groundwater. The freeze–thaw cycle in the active layer significantly impacts soil water
56 movement direction, velocity, storage capacity, and hydraulic conductivity (Bui et al., 2020;
57 Gao et al., 2021).

58 Frozen-soil hydrology attracts increasing attention, as the cold regions, e.g. Tibetan Plateau
59 and Arctic, are undergoing rapid changes (Tananaev et al., 2020). Frozen-soil thawing also
60 poses great threats to the release of frozen carbon in both high altitude and latitude
61 regions, which is likely to create substantial impacts on the climate system (Wang et al.,
62 2020). Attention is also growing for the impact of frozen-soil hydrology on nutrient
63 transport and organic matter, and frozen soil–climate feedback (Tananaev et al., 2020).
64 Hence, there are strong motivations to better understand frozen-soil hydrological processes
65 (Bring et al., 2016).

66 Frozen-soil degradation and its impact on hydrology is one of the research frontiers for the
67 hydrologic community (Blöschl et al., 2019; Zhao et al., 2020; Ding et al., 2020). “How will
68 cold region runoff and groundwater change in a warmer climate?” was identified by the
69 International Association of Hydrological Sciences (IAHS), as one of the 23 major unsolved
70 scientific problems (Blöschl et al., 2019), which requires stronger harmonization of
71 community efforts.



72 1.2 The frontier of frozen-soil hydrology

73 Knowledge on frozen-soil hydrology was acquired through detailed investigations at
74 isolated locations over various time spans by hydrologists and geocryologists (Woo et al.,
75 2012; Gao et al., 2021). At the core scale, there are many measurements of soil profiles,
76 including but not limited to soil temperature (Kurylyk et al., 2016; Han et al., 2018), soil
77 moisture (Dobinski, 2011; Chang et al., 2015), groundwater fluctuation (Ma et al., 2017;
78 Chiasson-Poirier et al., 2020), and active layer seasonal freeze-thaw processes (Wang et al.,
79 2016; Farquharson et al., 2019). At the plot/hillslope scale, land surface energy and water
80 fluxes are measured by eddy covariance, large aperture scintillometer (LAS), lysimeter, and
81 multi-layers meteorological measurements. Geophysical detection technology allows us to
82 measure various subsurface permafrost features. At the basin scale, except for traditional
83 water level and runoff gauging, water sampling and the measurements of isotopes and
84 chemistry components provide important complementary data to understand catchment
85 scale hydrological processes (Streletskiy et al., 2015; Ma et al., 2017; Yang et al., 2019).
86 Remote sensing technology, including optical, near- and thermal-infrared, passive and
87 active microwave remote sensing, has been used to identify surface landscape features (e.g.
88 vegetation and snow cover) and directly or indirectly retrieve subsurface variables (e.g.
89 near-surface soil freeze/thaw and permafrost state) in frozen-soil regions (Nitze et al., 2018;
90 Jiang et al., 2020).

91 Besides measurement, modeling provides another indispensable dimension to understand
92 frozen-soil hydrology in an integrated way, and make predictions in climate change. There
93 has been a revival in the development of frozen-soil hydrological models simulating
94 coupled heat and water transfer. Such physically-based models typically calculate seasonal
95 freeze-thaw through solving heat transfer equations. Such equations are either solved
96 analytically or numerically (Walvoord and Kurylyk, 2016). The Stefan equation is a typical
97 example of the analytical approach, which calculates the depth from the ground surface to
98 the thawing (freezing) horizon by the integral of ground surface temperature and soil
99 features. The Stefan equation is widely used to estimate active layer thickness (Zhang et al.,
100 2005; Xie and Gough, 2013), and is incorporated into some hydrological models (Wang L,
101 2010; Fabre et al. 2017). The numerical solution schemes (e.g., finite difference, finite
102 element, or finite volume) to model ground freezing and thawing, is typically applied to
103 one-dimensional infiltration into frozen soils, and is included in models such as SHAW (Liu
104 et al., 2013), CoupModel (Zhou et al., 2013), the distributed water-heat coupled (DWHC)
105 model (Chen et al. 2018), the distributed ecohydrological model (GBEHM) (Wang Y. 2018),
106 and the three-dimensional SUTRA model (Evans et al. 2018). Andresen et al (2020)
107 compared 8 permafrost models on soil moisture and hydrology projection across the major
108 Arctic river basins, and found that most models project a long-term drying of surface soil,
109 but the projection vary strongly in magnitude and spatial pattern. Except for hydrological
110 models, many land surface models explicitly consider the freeze-thaw process, in order to
111 improve land surface water and energy budget estimation and weather forecasting accuracy
112 in frozen-soil areas. Such models include VIC (Cuo et al., 2015), JULES (Chadburn et al.,
113 2015), CLM (Niu et al., 2006; Oleson et al., 2013; Gao et al., 2019), CoLM (Xiao et al., 2013),



114 Noah-MP (Li et al., 2020), ORCHIDEE (Gouttevin et al., 2012). Comprehensive reviews on
115 frozen-soil hydrological models can be found in Walvoord and Kurylyk (2016), Jiang et al.
116 (2020), and Gao et al. (2021).

117 1.3 The challenge of frozen-soil hydrological modeling

118 Although numerous frozen-soil hydrological models were developed, most models have
119 strong prior assumptions on the impacts of frozen-soil on hydrological behavior (Walvoord
120 and Kurylyk, 2016; Gao et al., 2021). Such models follow a "bottom-up" modeling approach,
121 which presents an "upward" or "reductionist" philosophy, based on the aggregation of
122 small-scale processes and *a priori* perceptions (Jarvis, 1993; Sivapalan et al., 2003). However,
123 most of the "upward" process understanding has been obtained from in-situ observation
124 and in-situ modeling, which have limited spatial and invariably limited temporal coverage
125 (Brutsaert, and Hiyama, 2012). It is worthwhile to note that frozen-soil has tremendous
126 spatial-temporal heterogeneities, which are strongly influenced by many intertwined factors,
127 including but not limited to climate, topography, geology, soil texture, snow cover, and
128 vegetation. Upscaling could average out some variables, and turn other variables visible and
129 even become dominant processes (Fenicia and McDonnell, 2022). Unfortunately, translating
130 spot/hillslope scale frozen-soil process to its influence on catchment scale hydrology,
131 guided by carefully expert analysis, and constrained by multi-source measurements, is still
132 largely unexplored.

133 The effects of the soil freeze/thaw process on hydrology at catchment scale is still
134 inconclusive. In the headwaters of the Yellow River, some modeling studies concluded that
135 permafrost has significant impact on streamflow (Sun et al., 2020). But in Sweden and the
136 northeast of the United States, other studies found frozen soil have negligible impact on
137 streamflow (Shanley and Chalmers, 1999; Lindstrom et al., 2002). Some studies found that
138 the impact of frozen soil on streamflow is concentrated in certain periods. For example,
139 Osuch et al. (2019) found permafrost to impact on groundwater recession and storage
140 capacity of the active layer in Svalbard island; Nyberg et al. (2001) found that in the Vindeln
141 Research Forest in northern Sweden permafrost impacted streamflow only in springs.
142 Hence, we argue that the impact of local scale freeze-thaw process on runoff should be
143 regarded as a hypothesis to be verified or rejected.

144 The unexplored frozen-soil hydrology is especially true for mountainous Asia, due to the
145 lack of long-term observations as a result of the difficulty of access and high cost of
146 operation. The cold region of the Tibetan Plateau is characterized by relatively thin and
147 warm frozen-soil with low ice content, due to the unique environmental conditions, arid
148 climate, high elevation and steep geothermal gradient (Cao et al., 2019; Zhao et al., 2020;
149 Jiang et al., 2020). Snow cover is thinner, and vegetation cover is poorer than in Arctic
150 regions. These features limit the insulation effect on freeze-thaw processes, resulting in a
151 much larger active layer depth (Pan et al., 2016). Topographical features, including elevation
152 and aspect, are major factors affecting permafrost distribution. The complex mountainous
153 terrain, as a result of recent tectonic movement, leads to large spatial heterogeneity in the
154 energy and water balance, and underexplored frozen-soil hydrology on the Tibetan Plateau



155 (Gao et al., 2021).

156 1.4 Aims and scope

157 In this study, we utilized a "top-down" approach (Sivapalan et al., 2003), to understand the
158 effect of frozen-soil on hydrology in the Hulu catchment on the northeastern edge of the
159 Tibetan Plateau. The aims of this study are as below:

- 160 1) Diagnosing the impacts of frozen-soil on hydrology in the mountainous Hulu
161 catchment, with multi-source, multi-scale data and model discrepancy;
- 162 2) Developing a quantitative conceptual frozen-soil hydrological model, based on expert-
163 driven interpretation in the form of perceptual model for the Hulu catchment;
- 164 3) Testing the realism of the conceptual frozen-soil hydrological model, with multi-source
165 and multi-scale observations.

166 In this paper, we firstly introduced the study site and data in Section 2; an expert-driven
167 perceptual frozen-soil hydrology model was proposed in Section 3; a semi-distributed
168 conceptual frozen-soil hydrological model, FLEX-Topo-FS, was developed in Section 4; the
169 realism of the FLEX-Topo-FS model was tested in Section 5; in Section 6 and 7, last but not
170 least, we made discussions and draw the conclusions.

171 2 Study site and data

172 The Hulu catchment (38°12'–38°17' N, 99°50'–99°54'E) is located in the upper reaches of
173 the Heihe River basin, the northeast edge of the Tibetan Plateau in northwest China (Figure
174 1). The elevation ranges from 2960 to 4820 m a.s.l., gradually increasing from north to south
175 (Figure 1) (Chen et al., 2014; Han et al., 2018). Most precipitation occurs in the summer
176 monsoon time, and snowfall in winter is limited (Han et al., 2018; Jiang et al., 2020). There is
177 a runoff gauging station at the outlet, controlling an area of 23.1 km². Two minor tributaries
178 are sourced from glaciers (east) and moraine-talus (west) zones, which merge at the
179 catchment outlet. The Hulu catchment has rugged terrain and very little human disturbance.
180 We identified four main landscape types, i.e. glaciers (5.6%), alpine desert (53.5%), vegetation
181 hillslope (37.5%), and riparian zone (3.4%) (Figure 2).

182 The Hulu catchment mostly extends on seasonal frozen-soil and permafrost (Zou et al.,
183 2014; Ma et al., 2021). Field survey in the upper Heihe revealed that the lower limit of
184 permafrost was 3650m~3700m (Wang et al., 2013), above that elevation is permafrost, and
185 below is seasonal frozen-soil. In the Hulu catchment, the lower limit of permafrost is around
186 3650m (Figure 1). Permafrost covers 64% of the catchment area, and the seasonal frozen-
187 soil covers 36%. There is a strong co-existence between soil freeze-thaw feature and
188 landscape (Figure 1). Permafrost and moraine/talus with poor vegetation cover co-exist in
189 higher elevation, with large heat conductivity and less heat insulation in winter, resulting
190 deep frozen depth. The seasonal frozen soil in relative lower elevation has better vegetation
191 cover, with better heat insulation and less heat conductivity in winter, resulting in shallower



192 frozen depth.

193 The elevation of the hydrometeorological gauging station is 2980m. We collected daily
194 runoff, daily average 2m air temperature, and daily precipitation from January 1st 2011 to
195 December 31st 2014. There was a flood event in 2013, which damaged the water level
196 sensor, resulted in a runoff data gap from June 17th to July 10th in 2013. Soil moisture was
197 measured in 20cm, 40cm, 80cm, 120cm, 180cm, 240cm, and 300cm depths from October 1st
198 2011 to December 31st 2013, with a data gap between August 3rd 2012 and October 2nd
199 2012. In the same soil moisture site, we also observed the soil freeze/thaw depth from 2011
200 to 2014. Groundwater depth was measured at WW01 site by four wells, with depth of 5m,
201 10m, 15m, and 25m respectively (Pan et al., 2021). The observation period was from 2016 to
202 2019, not overlaid with other hydrometeorological variables. Hence, we merely used the
203 groundwater level to qualitatively constrain and test our perceptual model.

204 **3 An expert-driven perceptual frozen-soil hydrology model**

205 **based on field observations**

206 Perceptual model is increasingly recognized as the central importance in hydrological
207 model development (Fenicia and McDonnell, 2022). Although perceptual model is a
208 qualitative representation of hydrological system, it bridges the gap between
209 experimentalists and modelers, and hold the base for quantitative conceptual model. In this
210 study, we developed a perceptual frozen-soil hydrology model for the Hulu catchment,
211 based on field measurements and our expertise.

212 **3.1 Observation1: Low runoff in the early thawing season (LRET)**

213 Precipitation-runoff time series analysis is a tradition and powerful tool to understand
214 catchment hydrology. When we plot Hulu catchment's precipitation and runoff data
215 together, we observed an interesting low runoff in the early thawing season (LRET)
216 phenomenon (Figure 3). For example, on June 5-9, 2013, there was a 45.7mm rainfall event,
217 with air temperature ranging from 3.0°C to 11.9°C, but with only 0.68mm in total runoff
218 generation. Ma et al., (2021) also showed that in the warm middle June 2015 in Hulu
219 catchment, there was a large rainfall event (over 30mm/d), but no runoff response was
220 observed. Moreover, this LRET phenomenon repeatedly happens every year, which allows
221 us to exclude the possibility of measurement errors.

222 To further investigate the LRET phenomenon, we plot the time series of observed daily
223 precipitation, temperature, runoff, freeze/thaw front depth, and soil moisture profile (20cm,
224 120cm, and 240cm) together (Figure 3). Soil moisture data showed that top soil was dry at
225 the beginning of thawing season. Gradually, soil was thawing from both topsoil and
226 downwards (Figure 3), and simultaneously the soil moisture was increased also downwards.
227 Although the topsoil was thawed, there was still frozen-soil underneath (Figure 3). The



228 water above the frozen-soil layer was even saturated with ponding but no percolation and
229 runoff generation. Moreover, the groundwater level further declined (Figure 12). This
230 illustrated that, during this period, the soil and groundwater system were disconnected, very
231 likely because the frozen soil blocked the percolation. As revealed by isotope data in the
232 Hulu catchment, groundwater contributed the dominant streamflow, i.e. 95% during the
233 frozen period (Ma et al., 2021). Thus, during this process, there was almost no runoff
234 generation, and the only contribution to streamflow during this period was the discharge
235 from groundwater system as baseflow. Our field work experience also verified that in the
236 early thawing season, vehicles were easy to be trapped in mires, because the surface soil
237 was muddy, saturated even over-saturated with ponding. When frozen-soil was complete
238 thaw in summer, trafficability became much better.

239 When completely thawed, the bidirectional thaw fronts meet, the soil moisture in the
240 bottom of frozen soil (around 2.4m in this study site, Figure 3) was increased sharply, and
241 then decreased, with a short period pulse. We also noted that the observation sites of
242 freeze/thaw front depth and soil moisture were both near the outlet of the Hulu catchment
243 in lower elevation (Figure 1). This means once the frozen soil in lower elevation was thawed,
244 soil and groundwater systems were reconnected. Hydrological processes, including
245 groundwater percolation and runoff generation, became the same as normal free of frozen-
246 soil circumstances.

247 **Learning from paired catchments**

248 The LRET phenomenon was widely documented in other cold regions (Figure 4), including
249 but not limited to the headwater of Yellow River (Yang et al., 2019), and the Cape Bounty
250 Arctic Watershed Observatory, Melville Island, NU in Canada (Lafrenière and Lamoureux,
251 2019). For example, at the headwater of Yellow River, on July 8-9 2014, there was a 21.9mm
252 rainfall event with temperature of 6.5°C, but little 1.5m³/s runoff; and on July 21-23 2014,
253 there was a 27.4mm rainfall event with temperature of 7.2°C, but only 5.1m³/s runoff.
254 Lafrenière and Lamoureux (2019) found that the undisturbed frozen soil at Cape Bounty
255 Arctic Watershed Observatory had little runoff generation in the early thawing season. But
256 after the frozen-soil was disturbed, the runoff response to rainfall event was much larger.
257 Hence this paired catchment study illustrated that frozen soil played a key role causing the
258 LRET phenomenon.

259 **3.2 Observation2: Discontinuous baseflow recession (DBR)**

260 Baseflow recession provides an important source of information to infer groundwater
261 characteristic, including its storage properties, subsurface hydraulics, and concentration
262 times (Brutsaert and Sugita, 2008; Fenicia et al., 2006), which is especially true for basins with
263 frozen-soil (Gao et al., 2021).

264 Baseflow analysis is based on the water balance equation (Equation 1), and linear reservoir
265 assumption (Equation 2). It should be noted that Equation 1 assumes no additional inflows
266 (recharge or thawing) or outflow (capillary rise or freezing). If a reservoir is linear, this
267 implies that the reservoir discharge (Q) has a linear relationship with its storage (S). K_s (days)



268 is time-constant controlling the speed of recession in the linear reservoir. With a larger K_s
269 value, the reservoir empties slower, and vice-versa. Combining Equation 1 and 2, we can
270 derive equation 3, illustrating how discharge depends on time (t), proportional to the initial
271 discharge (Q_0).

$$272 \quad \frac{dS}{dt} = -Q \quad (1)$$

$$273 \quad Q = S/K_s \quad (2)$$

$$274 \quad Q = Q_0 \cdot e^{-t/K_s} \quad (3)$$

275 **Baseflow recession analysis results**

276 In Figure 5, we plot the groundwater recession on semi-logarithmic scale. In the beginning
277 of freezing season, baseflow presented a clear linear recession, and was able to be fitted by
278 setting the recession coefficient (K_s) as 80 days. However, interestingly, simultaneously with
279 the LRET phenomenon, we observed a clear discontinuous baseflow recession in the Hulu
280 catchment (Figure 5). The baseflow bended down, and K_s became 60 days in the end of
281 recession periods. This DBR phenomenon informed us that the groundwater system had
282 additional outflow, and the groundwater storage was disturbed. We also noted the spikes
283 during the thawing in Fig. 5, which means groundwater was suddenly released. To our best
284 knowledge, these discontinuous baseflow recession (DBR) phenomenon is a new
285 observation for mountainous frozen-soil hydrology.

286 We also plot the variation of groundwater depth of 4 wells at WW01 site from 2016 to 2019
287 (Figure 1, 12). The wells of 5m, 10m, and 15m only had liquid water in thawing seasons, and
288 gradually went dry in recession periods. The water level of the 25m well was decreasing in
289 the entire frozen seasons, but in a discontinuous way. From the observed groundwater
290 depth, the groundwater level decreases faster at beginning. And after the groundwater level
291 dropped below around 17m, the decrease of groundwater level became slower. The turning
292 point from $K_s=80d$ to $K_s=60d$ occurred simultaneously while the groundwater level went
293 down to 17m (Figure 5, 12). The bending down discontinuous baseflow recession and
294 slower decrease of groundwater level indicated that there was a disturbance reduced the
295 groundwater discharge and lead to a slower decrease of groundwater level.

296 **Learning from paired catchments**

297 Frozen-soil is able to disturb the groundwater system, by freezing the liquid groundwater to
298 reduce groundwater storage, and leading to the DBR. But the DBR could also be caused by
299 many other reasons, for instance soil evaporation, root tapping, capillary rise, impermeable
300 layer, and heterogenous hydraulic conductivities in different landscapes (riparian area and
301 hillslope). Since the DBR phenomenon started from the middle of freezing period, and
302 lasted until the end of frozen season, in which time the evaporation, root tapping, and
303 capillary rise were very inactive even totally stopped, which allows us to exclude these
304 impacts. The impermeable layer and heterogenous hydraulic conductivities are both able to
305 result in discontinuous recession in small scale.

306 To further understand the DBR phenomenon, we collected larger scale runoff data in this



307 region, including the Zhamashike (5526 km²) and Qilian (2924 km²), which are also the sub-
308 basins of the upper Heihe. The permafrost and seasonal frozen-soil map of the upper Heihe
309 River basin shows that: the Zhamashike sub-basin has 74% permafrost and 26% seasonal
310 frozen soil, which is similar to the Hulu catchment; while the Qilian sub-basin has much less
311 permafrost area (38%), and is mostly covered by seasonal frozen-soil (62%) (Figure 1).

312 Interestingly, when plotting the hydrographs of these two sub-basins on logarithmic scale,
313 we can clearly see that in the permafrost dominated Zhamashike sub-basin discontinuous
314 recessions occurred, with $K_s=60d$ in the early and $K_s = 20d$ in the end of the recession
315 period. This DBR phenomenon is the same as we found in the Hulu catchment, although the
316 Zhamashike and Hulu catchment have quite different scales (5526 km² versus 23.1 km²)
317 (Chen et al. 2018, Gao et al., 2014). On the other hand, of similar size as the Zhamashike, the
318 Qilian sub-basin (2924 km²), which is mostly covered by seasonal frozen-soil, only has one
319 continuous recession, with $K_s = 60d$. The results from these two paired catchments provided
320 good reasons to interpret the DBR phenomenon in the Hulu catchment as the result of
321 frozen-soil.

322 3.3 Perceptual frozen-soil hydrology model of Hulu catchment

323 We did an expert-driven data analysis of the LRET and DBR observations, including time
324 series analysis of precipitation-runoff, soil moisture profile, freeze/thaw depth, and paired
325 catchments comparison. These comprehensive data analyses allowed us to identify that
326 both the LRET and the DBR were the results of frozen-soil, and motivated the following
327 perceptual model (Figure 7).

328 In the freezing season, at local scale, frozen soil occurs from the top soil downwards. But at
329 catchment scale, the freezing process does not occur in a homogeneous way. Since the
330 higher elevation is colder than the lower elevation, the freezing process starts from higher
331 elevation and downwards. At the beginning of the freezing season, although the top soil is
332 already frozen, the groundwater discharge from the supra-permafrost layer still continues. It
333 was found that the groundwater recession from the supra-permafrost layer determines the
334 dominant part of baseflow in permafrost regions (Brutsaert and Sugita, 2008; Ma et al.,
335 2021). Thus, the baseflow recession, during this period, appears not to be influenced by
336 frozen topsoil, and maintains a linear recession pattern, with $K_s=80d$ in the Hulu catchment.
337 With the increase of frozen depth, groundwater in the supra-permafrost layer is frozen
338 gradually from higher to lower elevation, which would gradually and dramatically reduce
339 groundwater discharge.

340 In the frozen season, the hydrological processes in the topsoil are almost completely
341 blocked, while in the permafrost region, the groundwater in the supra-permafrost layer is
342 largely inactive. But because there is still unfrozen liquid water in the frozen soil (Figure 3),
343 the model should also allow a small amount of liquid water to exist.

344 During the early thawing season, after a long groundwater recession, the groundwater level
345 is deep; and due to soil evaporation in winter, soil is dry and deficit of moisture.
346 Observations show that with the progress of thawing, soil temperature and soil moisture



347 increase from top to bottom, and the thawing front deepens downward. Rainfall firstly
348 infiltrates to saturate the moisture deficit without runoff generation. Moreover, the existence
349 of the impermeable deeper frozen-soil layer leads to vertical disconnection between soil
350 water and groundwater. Although there is probably saturated water above the frozen soil
351 (Figure 3 and 7), the poor vertical connectivity largely hinders soil water percolation.
352 Without recharge to groundwater, there is limited runoff generation during the early
353 thawing.

354 At the end of the thawing season, as soon as the thaw depth reaches its maximum or
355 frozen-soil no longer exists, the frozen groundwater is released. The spikes in the observed
356 hydrograph is likely due to different parts of the catchment reaching breakthrough, which
357 happens first in the lower elevations and then gradually moves upward to higher landscape
358 elements. This would trigger a sequence of sudden groundwater release and the spikes.
359 Snowfall is probably another influencing factor, causing the LRET and the spikes
360 phenomenon by storing precipitation as snow cover to reduce runoff, and releasing melting
361 water in a short time. This hypothesis needs to be tested by including snow accumulation
362 and melting processes in the hydrological model.

363 Once the soil is completely thawed at the end of the melting season, the rainfall-runoff
364 process returns to normal, and free of influence by the frozen-soil. Hence in the Hulu
365 catchment, frozen soil mainly impacts on streamflow during the freezing, frozen and
366 thawing periods.

367 Based on this perceptual model, we developed the conceptual framework of the frozen-soil
368 hydrological model, which needs to at least to consider the following elements: 1) we need
369 a semi-distributed modeling framework; 2) distributed forcing should be considered. 3)
370 different landscapes should be included; 4) topography should be involved, particularly
371 elevation; 5) we need to consider soil freeze/thaw processes; 6) snowfall and melting should
372 be included; 7) glacier melting should be included; 8) last but not least, the normal rainfall-
373 runoff processes are still important, because most runoff happen in the warm season, which
374 functions the same as in temperate climate regions.

375 **4 A semi-distributed conceptual frozen-soil hydrology model**

376 The perceptual model requires a quantitative conceptual model to test, revise, polish, verify,
377 or even reject its hypotheses. Since the Hulu catchment has heterogenous landscapes, with
378 a large elevation gradient, diverse land cover, and complex freeze/thaw process, we
379 developed a semi-distributed frozen-soil hydrological model, i.e. FLEX-Topo-FS, based on
380 the landscape-based hydrological modeling framework, i.e. FLEX-Topo. Numerous
381 processes were involved in FLEX-Topo, including the distributed meteorological forcing,
382 landscape heterogeneity, and snow and glacier melting. And in FLEX-Topo-FS, we explicitly
383 considered the impacts of frozen-soil on soil water percolation and groundwater frozen
384 processes in the supra-permafrost layer. The details of both the FLEX-Topo model (without
385 frozen soil) and FLEX-Topo-FS model (with frozen soil) are described in below.



386 4.1 FLEX-Topo model (without frozen-soil)

387 4.1.1 Catchment discretization and meteorological forcing interpolation

388 The FLEX-Topo model classified the entire Hulu catchment into four landscapes, i.e. glaciers,
389 alpine desert, vegetation hillslope, and riparian zone. The Hulu catchment (from 2960m to
390 4820m) was classified into 37 elevation bands, with 50m interval (Figure 2). Combined 4
391 landscapes and 37 elevation bands, we had $37 \times 4 = 148$ hydrological response units (HRUs).
392 The structure of FLEX-Topo model consisted of four parallel components, representing the
393 distinct hydrological function of different landscape elements (Savenije, 2010; Gao et al.,
394 2014; Gharari et al., 2014; Gao et al., 2016). And the corresponding discharge of all elements
395 was subsequently aggregated to obtain the simulated runoff.

396 We interpolated the precipitation (P) and temperature (T) based on elevation bands from
397 in-situ observation (2980m) to each elevation band. The precipitation increasing rate was
398 set as 4.2%/100m, and temperature lapse rate as $-0.68^\circ\text{C}/100\text{m}$, based on field
399 measurements (Han et al., 2013). Snowfall (P_s) or rainfall (P_r) was separated by air
400 temperature, with the threshold temperature as 0°C (Gao et al., 2020).

401 4.1.2 Model description and configuration

402 FLEX-Topo is a semi-distributed conceptual bucket model (Savenije, 2010; Gao et al., 2014),
403 with three modules, i.e. the snow and glacier module, the rainfall-runoff module, and the
404 groundwater module. The water balance and constitutive equations can be found in Table 1.
405 The model parameters and their prior ranges for calibration are listed in Table 2.

406 Snow and glacier module

407 The temperature-index method was employed to simulate snow and glacier melting (Gao et
408 al., 2020). We used a snow reservoir (S_w) to account for the snow accumulating, melting (M_w)
409 and water balance (Equation 4). The snow degree-day factor (F_{3d}) needs to be calibrated.
410 For glaciers, we assumed its area was constant in our simulation (from 2011 to 2014).
411 Glacier melting (M_g) was also calculated by the temperature-index method (Equation 7), but
412 with different degree-day factor. With the same air temperature, glacier has less albedo
413 than snow cover, thus with larger amount of melting. Glacier degree-factor was obtained by
414 multiplying snow degree-day factor (F_{3d}) with a correct factor C_g (Equation 8) (Gao et al.,
415 2020).

416 Rainfall-runoff module

417 There are two reservoirs to simulate rainfall-runoff process, including the root zone
418 reservoir (S_r) (Equation 10) and fast response reservoir (S_f) (Equation 17). To account of the
419 different rainfall-runoff processes in different landscapes and simultaneously avoid over
420 parameterization, we kept the same model structure for vegetation hillslope, riparian and
421 alpine desert (Equation 11, 12), but gave different root zone storage capacity (S_{rmax}) values,
422 i.e. $S_{rmax,R}$ for riparian, $S_{rmax,D}$ for cold desert, and $S_{rmax,V}$ for hillslope vegetation. For vegetation



423 hillslope, a larger prior range was constrained for the root zone storage capacity ($S_{\text{max},V}$),
424 which means more water is required to fill in its storage capacity to meet its water deficit,
425 which is evidenced by previous studies in this region (Gao et al., 2014). For alpine desert,
426 due to its sparse vegetation cover, we constrained a shallower root zone storage capacity
427 ($S_{\text{max},D}$). For the riparian area, due to its location where is prone to be saturated, we also
428 constrained a shallower root zone storage capacity ($S_{\text{max},R}$). The initial states (beginning of
429 2011) of the reservoirs were obtained from the end values (end of 2014) of the simulation,
430 which is a normal procedure in modeling practice.

431 Other parameters in rainfall-runoff module (Equation 11-18, Table 1) include the threshold
432 value controlling evaporation (C_e), the shape parameter of the root zone reservoir (β), the
433 splitter (D) separating the generated runoff (R_i) from the root zone reservoir (S_i) to the fast
434 response reservoir, the recession parameter of faster reservoir (K), and the lag time from
435 rainfall event to peak flow ($T_{\text{lag}F}$). We set D as 0.2 from the isotope study (Ma et al., 2021).
436 And other parameters to be calibrated, with prior ranges (Table 2) based on previous
437 studies (Gao et al., 2014; Gao et al., 2020).

438 **Groundwater module**

439 The baseflow (Q_s) is generated from groundwater recession. The groundwater was
440 simulated by a linear reservoir (S_s) described in Section 3.2, and Equation 19. We set the
441 prior range for recession coefficient of baseflow reservoir (K_s) as (10-100 d). To estimate the
442 impacts of frozen groundwater on hydrological processes, we set the groundwater in
443 different landscapes as parallel. But we analyzed groundwater level as an integrated system,
444 because groundwater system is connected and this affects the groundwater level. Since the
445 sub-permafrost groundwater is even deeper than 20m in the Hulu catchment, and almost
446 disconnected to streamflow, thus we only model the supra-permafrost groundwater.

$$447 \quad Q_s = S_s / K_s \quad (19)$$

448 **4.2 FLEX-Topo-FS model (with frozen soil)**

449 **4.2.1 Modeling the soil freeze/thaw processes**

450 FLEX-Topo-FS model employed the Stefan equation (Equation 20), to provide an
451 approximate solution to estimate freeze/thaw depth (Figure 10). The Stefan equation is a
452 temperature-index based freeze-thaw algorithm, which assumes the sensible heat is
453 negligible in soil freeze/thaw simulation (Xie and Gough, 2013). The form of Stefan equation
454 is written as:

$$455 \quad \varepsilon = \left(\frac{2 \cdot 86400 \cdot k \cdot F}{Q_L} \right)^{0.5} = \left(\frac{2 \cdot 86400 \cdot k \cdot F}{L \cdot \omega \cdot \rho} \right)^{0.5} \quad (20)$$

456 where ε is the freeze/thaw depth; k is the thermal conductivity ($W/(m \cdot K)$) of the soil; F is the
457 surface freeze/thaw index. Freeze index ($^{\circ}C$ degree-days) is the accumulated negative



458 ground temperature, while freezing; thaw index ($^{\circ}\text{C}$ degree-days) is accumulated positive
459 ground temperature, while thawing. Q_L is the volumetric latent heat of soil, in J/m^3 ; and
460 $Q_L = L \cdot \omega \cdot \rho$ where L is the latent heat of fusion of ice ($3.35 \cdot 10^5 \text{ J}/\text{kg}$); ω is the water
461 content, as a decimal fraction of the dry soil weight; and ρ is the bulk density of the soil
462 (kg/m^3).

463 We set the thermal conductivity as $k=2 \text{ W}/(\text{m}\cdot\text{K})$, the water content as a decimal fraction of
464 the dry soil weight $\omega = 0.12$, and bulk density of the soil $\rho=1000 \text{ kg}/\text{m}^3$ (Zhang et al.,
465 2019). Since the Stefan equation requires ground surface temperature, which is difficult to
466 measure and often lack of data, we used a multiplier to translate the air temperature to
467 ground temperature. The multiplier during freezing was set as 0.6, and during thawing we
468 assumed the ground surface temperature was the same as air temperature (Gisnås et al.,
469 2016).

470 In this model, we did not consider the impacts of snow cover on soil freeze/thaw, because
471 the snow effects were compiled in the Hulu catchment. Firstly, because precipitation in the
472 Hulu catchment mostly happens in summer as rainfall, and snow depth in the Hulu
473 catchment was less than 10mm in most area and time. Secondly, the snow cover has
474 contrary effects on ground temperature. Snow cover as an isolation layer increased ground
475 temperature in winter. But simultaneously snow cover also increased albedo, which
476 decreased net radiation, and decreased ground temperature. To avoid over
477 parameterization, we did not consider snow effect in the Stefan equation.

478 In this study, the Stefan equation was driven by distributed air temperature, which allowed
479 us to simulate the distributed soil freeze/thaw processes. With the distributed soil freeze
480 index and thaw index, we can also estimate the lower limit of permafrost, of which elevation
481 the freeze index equals to the thaw index in mountainous regions. Field survey on the lower
482 limit of permafrost (Wang et al., 2016) can provide another strong confirmation to our
483 simulated soil freeze/thaw process, except for the spot-scale freeze/thaw depth.

484 4.2.2 Modeling the impacts of frozen-soil on hydrology

485 The distributed freeze/thaw status calculated by FLEX-Topo-FS model allowed us to
486 simulate the impacts of frozen-soil on soil and groundwater systems, their connectivity, and
487 eventually catchment runoff.

488 In freezing and frozen seasons, precipitation was in the phase of snowfall, and topsoil was
489 frozen, thus without surface runoff. During this period, runoff is only contributed from the
490 groundwater discharge of the supra-permafrost layer (Q_s). There is no runoff generation (R_i)
491 from the root zone reservoir to the response routine (S_s and S) in this period. In the
492 conceptual model, we set $R_i = 0$ (Equation 11). In freezing season, when frozen depth was
493 less than 3m (the depth of active layer in this region), the groundwater in the supra-
494 permafrost layer still functions, and was simulated by linear groundwater reservoir (S_s). Once
495 the frozen depth of certain elevation zone is larger than 3m, the groundwater in that
496 elevation zone was frozen (\bar{S}). In the FLEX-Topo-FS model, we reduced the groundwater
497 storage (S_s) to 10% of its total storage, to simulate its frozen status (Equation 21, 22). This



498 amount of frozen water (F_s , 90% of groundwater storage when frozen, marked as $S_s(\tilde{t})$)
499 does not disappear, but held in the groundwater system as frozen-soil (Equation 22). We
500 set 90% frozen, rather than 100%, because there is still unfrozen liquid water in frozen-soil.
501 Groundwater discharge was controlled by the frozen status, which was frozen from high
502 elevations to lower elevations. This process is like progressively stopping the function of a
503 series of cascade buckets, resulting in the discontinuous recession. Simultaneously, the
504 decrease of discharge (Q_s) slowed down the decrease of groundwater level (S_s). This
505 conceptual model allowed us to simulate the bend down of baseflow recession and slower
506 decreasing of groundwater level.

$$507 \quad \frac{dS_s}{dt} = R_s - Q_s - F_s \quad (21)$$

$$508 \quad F_s = \begin{cases} 0.9 \cdot S_s(\tilde{t}); & \text{once freeze depth} \geq 3m \\ -0.9 \cdot S_s(\tilde{t}); & \text{once thaw depth reach to yearly max} \\ & \text{or thaw depth} \geq \text{freeze depth} \end{cases} \quad (22)$$

509 In early thawing season, the freeze/thaw condition in the lowest elevation zone plays a key
510 role, controlling the hydraulic connectivity between soil and groundwater systems. In the
511 conceptual model, if freeze depth calculated by Stefan equation is larger than thaw depth,
512 this means the frozen layer still exists. In the conceptual model, we kept as the runoff
513 generation $R_o = 0$ (Equation 11). Since there is no percolation from soil to groundwater, and
514 root zone soil moisture (S_s) is accumulating, even ponding in some local depressions (Figure
515 7). The only outflow of the root zone is evaporation in this period. This conceptual model
516 allowed us to reproduce the LRET observation. For groundwater reservoir, once the thaw
517 depth goes to its yearly maximum (in permafrost area) or thaw depth > freeze depth (in
518 seasonal frozen-soil area), the frozen water (90% of groundwater storage when frozen,

519 $S_s(\tilde{t})$) was released to the groundwater again (Equation 22). The release of frozen
520 groundwater could happen in either thawing seasons or complete thaw seasons depending
521 on its elevation. But in either way, the water balance calculation is one-hundred-percent
522 closed.

523 Complete thaw in the lowest elevation marked the end of thawing season, and the start of
524 complete thaw season. In the complete thaw season, soil water and groundwater are
525 connected, and runoff generation (R_o) returns to normal circumstances, which can be
526 simulated by the FLEX-Topo model without frozen-soil.

527 4.3 Model uncertainty analysis and evaluation metrics

528 The Kling-Gupta efficiency (Gupta et al., 2009; KGE) was used as the performance metric in
529 model calibration:

$$530 \quad KGE = 1 - \sqrt{(r - 1)^2 + (\alpha - 1)^2 + (\beta - 1)^2} \quad (23)$$



531 Where r is the linear correlation coefficient between simulation and observation; α ($\alpha =$
532 σ_m/σ_o) is a measure of relative variability in the simulated and observed values, where σ_m is
533 the standard deviation of simulated variables, and σ_o is the standard deviation of observed
534 variables; β is the ratio between the average value of simulated and observed variables.

535 We applied the Generalized Likelihood Uncertainty Estimation framework (GLUE, [Beven and](#)
536 [Binley, 1992](#)) to estimate model parameter uncertainty. Sampling the parameter space with
537 20, 000 parameter sets, and select the top 1% parameter as behavioral parameter sets.

538 For a comprehensive assessment of model performance in validation, the behavioral model
539 runs were evaluated using multiple criteria, including KGE, KGL (the KGE of logarithms flow,
540 and more sensitive to baseflow), Nash-Sutcliffe Efficiency (NSE) ([Nash and Sutcliffe, 1970](#))
541 (Equation 24), coefficient of determination (R^2) and root mean square error (RMSE).

$$542 \quad NSE = 1 - \frac{\sum_{t=1}^n (Q_o - Q_m)^2}{\sum_{t=1}^n (Q_o - \overline{Q_o})^2} \quad (24)$$

543 Where Q_o is observed runoff, $\overline{Q_o}$ is the observed average runoff, and Q_m is modeled runoff.

544 The model was calibrated in the period 2011-2012, and uses KGE as objective function. The
545 second half time series (2013-2014) were used to quantify the model performance in
546 streamflow split-sample validation, with multi-criteria including KGE, KGL, NSE, R^2 , and
547 RMSE. The KGE, KGL, NSE and R^2 are all less than 1, and their valuation closer to 1 indicates
548 better model performance. While the less value of RMSE indicates less error and better
549 performance.

550 **5 Testing the realism of FLEX-Topo-FS model**

551 **5.1 FLEX-Topo model results and its discrepancy**

552 Figure 9 shows that the FLEX-Topo model can somehow reproduce the observed
553 hydrography in most periods, except for the LRET and DBR events. In calibration, the KGE
554 was 0.78. And in validation, the KGE =0.58, KGL =0.36, NSE =0.41, $R^2= 0.82$, and RMSE =
555 0.95mm/d. While taking account the impacts of landscape heterogeneity, the FLEX-Topo
556 model can to some extent simulate the LRET phenomenon. The vegetated hillslope in
557 relatively lower elevation has larger unsaturated storage capacity, with larger soil moisture
558 deficit in the beginning of melting season, and capable to hold more rainfall with initial dry
559 soil. Moreover, FLEX-Topo model has took snow accumulation and melting into account,
560 which also reduced the runoff generation during the LRET periods. However, there was still
561 large overestimation in the early thawing season.

562 Additionally, the simulated hydrography on logarithm scale clearly shows that the baseflow
563 is the result of a linear reservoir (Figure 9). The linear reservoir model can mimic recession
564 quite well in the beginning of baseflow recession, but the model discrepancy becomes



565 larger in the middle to the end of frozen season. Hence, FLEX-Topo model is not able to
566 simulate the discontinuous recession. The model discrepancy indicates that without
567 considering frozen-soil, FLEX-Topo cannot well reproduce the observed LRET and DBR
568 observations, although explicitly considered landscape heterogeneity, snow and glacier
569 processes.

570 5.2 FLEX-Topo-FS model results

571 5.2.1 Freeze/thaw simulation by FLEX-Topo-FS model

572 Figure 10 demonstrates that the Stefan equation was capable to reproduce the freeze/thaw
573 process. This verified the success of the freeze/thaw parameterization and the parameter
574 sets. Also, the simulated lower limit of permafrost is 3716m, which is largely close to field
575 survey in the upper Heihe River basin, around 3650 – 3700 m (Wang et al., 2016), and the
576 expert-driven estimation of 3650 m of Hulu catchment. Both the well reproduced
577 freeze/thaw variation in spot scale, and the lower limit of permafrost in catchment scale,
578 gave us strong confidence to the simulation of soil freeze/thaw processes.

579 5.2.2 Runoff simulation by FLEX-Topo-FS model

580 While considering the impacts of frozen-soil, the FLEX-Topo-FS model, compared with
581 FLEX-Topo, dramatically improved the model performance. Figure 11 showed the simulated
582 hydrograph by FLEX-Topo-FS on both normal and log scales. Both the LRET and the DBR
583 observations were almost perfectly reproduced by the FLEX-Topo-FS model. The KGE of
584 FLEX-Topo-FS in calibration was 0.78, which was the same as FLEX-Topo. But in validation,
585 the performance was significantly improved, the KGE improved from 0.58 to 0.66, KGL was
586 from 0.36 to 0.72, NSE was from 0.41 to 0.60, R^2 from 0.82 to 0.83, and RMSE was reduced
587 from 0.95mm/d to 0.79mm/d. All the model evaluation criteria were improved. The most
588 significant improvement was the baseflow simulation, and KGL was increased from 0.36 to
589 0.72. We also noted that the FLEX-Topo-FS model reproduced the spikes during the
590 thawing in Figure 11. This further confirms our conceptual model of a sequence of thawing
591 breakthroughs, which trigger the sudden release of groundwater starting at lower elevations
592 and progressing to higher landscape elements.

593

594 5.2.3 Modeling groundwater trends

595 To further verify the FLEX-Topo-FS model, we averaged the simulated groundwater storage
596 (S_s) of all HRUs, and compared with the observed groundwater depth on log scale (Figure
597 12). We included the frozen groundwater in the total groundwater storage (S_s), because the
598 liquid groundwater is in connection with the frozen groundwater and this affects the
599 groundwater level variation. Figure 12 clearly demonstrated that the simulated groundwater
600 storage decreased slower, and the time scale of recession was increased. The trends of



601 simulated groundwater storage and observed groundwater level, correspond surprisingly
602 well. This is particularly encouraging, given that the periods of simulation (2011-2014) and
603 observation (2016-2019) were not overlaid, and a point observation may not be
604 straightforwardly representative for the entire basin.

605 The success to reproduce groundwater level trends is another strong confirmation for the
606 FLEX-Topo-FS model. All the successes of FLEX-Topo-FS model to reproduce spot scale
607 freeze/thaw depth variation, lower limit of permafrost, LRET and DBR events, and
608 groundwater level trends, gave us strong confidence to the realism of our qualitative
609 perceptual model and quantitative conceptual model.

610 **6 Discussion**

611 **6.1 Diagnosing the impacts of frozen-soil on complex mountainous hydrology**

612 **6.1.1 Understanding complex frozen-soil hydrology by hydrography analysis**

613 Frozen-soil happens underneath, with frustrating spatial-temporal heterogeneities, and
614 difficulty to measure. Although there are spot and hillslope measurements, its impact on
615 catchment hydrology is still hard to explore. Hydrography, easily and widely observed and
616 globally accessible, can be regarded as the by-product of the entire catchment hydrological
617 system (Gao, 2015). Hydrography as an integrated signal provides us a vital source of
618 information, reflecting how the complex hydrological system works, i.e. transforming
619 precipitation into runoff. Hence, hydrography itself is a valuable source of data to
620 understand catchment frozen-soil hydrology.

621 Especially the baseflow embodies the influence of basin characteristics including the
622 geology, soils, morphology, vegetation, and frozen-soil (Blume et al., 2007; Ye et al., 2009).
623 Hence, the quantitative description of baseflow is a valuable tool for understanding how the
624 groundwater system behaves (McNamara et al., 1998). Baseflow recession was used to
625 identify the impacts of climate change on permafrost hydrology. In previous studies,
626 Slaughter and Kane (1976) found that basins with permafrost have higher peak flows and
627 lower baseflows. The baseflow, representing groundwater recession, provides important
628 information about the storage capacity and recession characteristics of the active layer in
629 permafrost regions (Brutsaert, and Hiyama, 2012).

630 Moreover, hydrological system has tremendous influencing factors. The hydrograph of
631 paired catchments provides a good reference, as a controlled experiment, to isolate one
632 influencing factor from the others. Nested catchments helped us to acknowledge the
633 importance of region-specific knowledge, which is often the key to interpret the
634 unexplained variability of large sample studies (Fenicia and McDonnell, 2022). In this study,
635 the pair catchment method helped us to confirm the impacts of frozen-soil on LRET and
636 DBR observations.



637 Moreover, by analyzing the nested sub-basins of the Lena River in Siberia, [Ye et al. \(2008\)](#)
638 used the peak flow/baseflow ratio to quantify the impact of permafrost coverage on
639 hydrograph regime in Lena River basin, and found that frozen-soil only affects discharge
640 regime over high permafrost regions (greater than 60%), and no significant affect over the
641 low permafrost (less than 40%) regions. In this study, we reconfirmed this statement. The
642 permafrost area proportions of the Hulu catchment and Zhamashike sub-basin are 64% and
643 74%, with significant effects on discharge, while 38% of the Qilian sub-basin is covered by
644 permafrost, with no significant effects on discharge regime.

645 By paired catchments comparison, interestingly, the K_s in Zhamashike and Qilian in the early
646 recession period are both 60d, which is exactly within the standard value of 45 ± 15 days
647 derived in earlier studies for basins ranging in size between 1,000 and 100,000 km²
648 ([Brutsaert and Sugita, 2008](#); [Brutsaert and Hiyama, 2012](#)), which was likely the results of
649 catchment self-similarity. But we also noticed that the K_s in the small Hulu catchment ($K_s =$
650 80d and 60d) is quite larger than the Zhamashike ($K_s = 60d$ and 20d) and Qilian ($K_s = 60d$).
651 This could be rooted in different scale and drainage density ([Brutsaert and Hiyama, 2012](#)).
652 The Hulu catchment is located in the headwater with less drainage density, hence less
653 contact area between hillslope and river channel, slower baseflow recession, and larger K_s
654 value. We argue that the validity of the standard value of K_s (45 ± 15 days), in small
655 catchments less than 1,000 km², may need more studies.

656 **6.1.2 Understanding complex frozen-soil hydrology by multi-source observations**

657 Observation is still a bottleneck in complex mountainous cold regions. Traditionally,
658 fragmented observations are only for specific variables, like puzzles. In this study, we
659 collected multi-source data, including soil moisture, groundwater level, topography,
660 geology survey, isotope, soil temperature, freeze/thaw depth, permafrost and seasonal
661 frozen-soil map, and hydrograph in paired catchments. Multi-source data analysis provides
662 multi-dimensional perspective to investigate frozen-soil hydrology. We argue that on one
663 hand, multi-source observations helped us to deliver the perceptual and conceptual
664 models. And on the other hand, perceptual and conceptual models bridge the gap between
665 experimentalists and modelers ([Seibert and McDonnell, 2002](#)), allowing us put fragmented
666 observations together, and understand the hydrological system in an integrated and
667 qualitative way.

668 Data gap is a common issue in mountainous hydrology studies. For example, in this study,
669 runoff data has a gap period in the end of thawing season in 2013, due to flooding and
670 equipment malfunction. Soil moisture and groundwater level data had large gap, which
671 cannot be used for continuous modeling. Luckily, the meteorological data, which is
672 important forcing data to run the models, was continuous without any gap. With sufficient
673 meteorological forcing data, we successfully run the hydrological models from 2011 to
674 2014. The runoff data gap in the end of thawing season in 2013 merely influenced model
675 validation. While evaluating models, we did not involve the data gap period. Hence, the
676 data gap does not have any impact on the consolidation of the conclusions.

677 In general, we argue that data gap always exists. In another words, we can never have



678 sufficient data. The only thing we can do is using the accessible data to understand
679 processes. In this study, although soil moisture had large gap, fortunately there were some
680 observations during the LRET periods, which were sufficient to distinguish the impacts of
681 frozen soil on soil moisture profile. Additionally, although the groundwater level observation
682 (2016-2019) was not overlaid with other hydrometeorological measurements (2011-2014),
683 its repeating seasonal pattern allowed us to qualitatively understand how groundwater
684 system behaves. We argue that perfect data does not exist, but with more multi-source and
685 better data quality, the more accurate understanding we can achieve. This needs the close
686 collaboration among multi-disciplinary researchers, including but not limited to
687 hydrologists, meteorologists, ecologists, geocryologists, geologists, and engineers.

688 **6.1.3 Understanding complex frozen-soil hydrology by model discrepancy**

689 By a simple water balance inspection, we found that the total annual runoff of Hulu
690 catchment was 499mm/a, which is even larger than the observed annual precipitation
691 433mm/a. This means that without considering distributed meteorological forcing, the
692 runoff coefficient is larger than 1, and the water balance cannot be closed. This result is also
693 in line with previous studies, showing that precipitation in mountainous areas is largely
694 underestimated (Immerzeel et al., 2015; Chen et al., 2018; Zhang et al., 2018b).

695 Although the semi-distributed FLEX-Topo has considered tremendous processes, including
696 rainfall-runoff processes, distributed forcing, landscape heterogeneity, topography, snow
697 and glacier melting, there was still model discrepancy to reproduce the LRET and DBR
698 observations. This means there must be some processes missed in the model. After our
699 expert-driven data analysis, we attributed the model discrepancy to soil freeze/thaw
700 processes.

701 Model fitness is the goal which all modelers are pursuing. But we argue that in many cases,
702 model discrepancy can tell us more interesting things than perfect fitting. In this study, we
703 used the FLEX-Topo model, without frozen-soil, as a diagnosing tool to understand the
704 possible impacts of frozen-soil on the complex mountainous hydrology. Using tailor-made
705 hydrological model and integrated observations as diagnostic tools is a promising approach
706 to step-wisely understand the complex mountainous hydrology.

707 **6.2 Modeling frozen-soil hydrology: top-down VS bottom-up**

708 Top-down and bottom-up are two philosophies for model development (Sivalpalan et al.,
709 2003). The bottom-up approach attempts to model catchment scale response based on the
710 prior knowledge learned in small scale. Bottom-up approach is commonly used in frozen-
711 soil hydrological modeling, because this is straightforward. And for modeling, it is a
712 common practice to experiment with/without a certain process, and claim its impacts on
713 runoff. But the bottom-up modeling largely missed the key step to diagnose the impacts of
714 small-scale processes on catchment response. Lack of process understanding usually leads
715 modeling studies to data pre- and pro-processing and extensive parameter calibration with
716 the risk of equifinality and model malfunction.



717 By our expert-driven top-down modeling approach, we firstly tried to understand the
718 hydrological processes at work, using multi-source data and analysing model discrepancy.
719 We then translated our understanding to perceptual and conceptual models. The top-down
720 method is an appealing way to identify the key influencing factors, rather than being lost in
721 endless detail and heterogeneities. Such informed analysis of the data helps to bring
722 experimentalist insights into the initiation of the conceptual model construction.

723 6.3 Climate change impacts on frozen-soil hydrology

724 To quantify the impacts of climate change on frozen-soil hydrology, we arbitrarily set the air
725 temperature increased by 2°C. The FLEX-Topo-FS simulation illustrated that complete thaw
726 date became 16-19 days earlier, and the lower limit of permafrost increased by 294 m, from
727 3716m to 4010m. For runoff simulation, the DBR phenomenon became less obvious (Figure
728 13). Both the baseflow and runoff in early thawing seasons were increased. This means
729 climate change will increase baseflow, which phenomenon was already widely observed in
730 Arctic and mountainous permafrost rivers (Ye et al., 2009; Brutsaert et al., 2012; Niu et al.,
731 2010). Hence, this result could be another verification for the FLEX-Topo-FS model realism.
732 For implications in water resource management, the results indicate that frozen soil
733 degradation caused by climate change may largely alter streamflow regime, especially for
734 the thirsty spring and early summer, in vast cold Tibetan Plateau. It is worthwhile to be
735 noted that this is very primary prediction. And we need more detailed studies to use the
736 state-of-the-art climate prediction and downscaling methodologies, to assess the frozen-
737 soil change and hydrology variations in future.

738

739 7 Conclusions

740 Our knowledge on frozen-soil hydrology is still incomplete, which is particularly true for
741 complex mountainous catchment on the Tibetan Plateau. In the past decades, we have
742 collected numerous heterogeneities and complexities in frozen-soil regions, but most of
743 these observations are still neither well integrated into hydrological models, nor used to
744 constrain model structure or parameterization in catchment-scale studies. More
745 importantly, we still largely lack quantitative knowledge on which variables play more
746 dominant roles at certain spatial-temporal scales, and should be included in models with
747 priority.

748 By conducting this frozen-soil hydrological modeling study for the complex mountainous
749 Hulu catchment, we reached the following conclusions: 1) we observed two new
750 phenomena in the frozen-soil catchment, i.e. the low runoff in early thawing seasons (LRET)
751 and discontinuous baseflow recession (DBR), which are widespread but not yet reported; 2)
752 without considering the frozen-soil, the FLEX-Topo model was not able to reproduce LRET
753 and DBR observations; 3) considering frozen-soil impacts on soil-groundwater connectivity,
754 and groundwater recession, the FLEX-Topo-FS model successfully reproduced the LRET and



755 DBR events. The FLEX-Topo-FS results were also verified by observed freeze/thaw depth
756 variation, groundwater level, and lower limit of permafrost. We believe this study is able to
757 give us new insights into further implications to understand the impact of frozen soil on
758 hydrology, projecting the impacts of climate change on water resources in vast cold regions,
759 which is one of the 23 major unsolved scientific problems in hydrology community.

760

761 **ACKNOWLEDGMENTS**

762 This study was supported by the National Natural Science Foundation of China (Grant Nos.
763 42122002, 42071081, 42171125, and 41971041).

764

765 **References:**

766 Andresen, C. G., Lawrence, D. M., Wilson, C. J., David McGuire, A., Koven, C., Schaefer, K.,
767 Jafarov, E., Peng, S., Chen, X., Gouttevin, I., Burke, E., Chadburn, S., Ji, D., Chen, G., Hayes, D.
768 and Zhang, W.: Soil moisture and hydrology projections of the permafrost region—a model
769 intercomparison, *Cryosphere*, 14(2), 445–459, doi:10.5194/tc-14-445-2020, 2020.

770 Beven, K. and Binley, A.: The future of distributed models: Model calibration and uncertainty
771 prediction, *Hydrol. Process.*, 6(3), 279–298, doi:10.1002/hyp.3360060305, 1992.

772 Blume, T., Zehe, E. and Bronstert, A.: Rainfall-runoff response, event-based runoff
773 coefficients and hydrograph separation, *Hydrol. Sci. J.*, 52(5), 843–862,
774 doi:10.1623/hysj.52.5.843, 2007.

775 Blöschl, G., Bierkens, M. F. P., Chambel, A., et al.: Twenty-three unsolved problems in
776 hydrology (UPH)—a community perspective, *Hydrol. Sci. J.*, 64(10), 1141–1158,
777 doi:10.1080/02626667.2019.1620507, 2019.

778 Bring, A., Fedorova, I., Dibike, Y., Hinzman, L., Mård, J., Mernild, S. H., Prowse, T., Semenova,
779 O., Stuefer, S. L. and Woo, M. K.: Arctic terrestrial hydrology: A synthesis of processes,
780 regional effects, and research challenges, *J. Geophys. Res. G Biogeosciences*, 121(3), 621–
781 649, doi:10.1002/2015JG003131, 2016.

782 Brutsaert, W. and Sugita, M.: Is Mongolia's groundwater increasing or decreasing? The case
783 of the Kherlen River basin, *Hydrol. Sci. J.*, 53(6), 1221–1229, doi:10.1623/hysj.53.6.1221,
784 2008.

785 Brutsaert, W. and Hiyama, T.: The determination of permafrost thawing trends from long-
786 term streamflow measurements with an application in eastern Siberia, *J. Geophys. Res.*
787 *Atmos.*, 117(22), 1–10, doi:10.1029/2012JD018344, 2012.

788 Bui, M. T., Lu, J. and Nie, L.: A review of hydrological models applied in the permafrost-
789 dominated Arctic region, *Geosci.*, 10(10), 1–27, doi:10.3390/geosciences10100401, 2020.

790 Cao, B., Zhang, T., Wu, Q., Sheng, Y., Zhao, L. and Zou, D.: Permafrost zonation index map



- 791 and statistics over the Qinghai–Tibet Plateau based on field evidence, *Permafr. Periglac.*
792 *Process.*, 30(3), 178–194, doi:10.1002/ppp.2006, 2019.
- 793 Chadburn, S., Burke, E., Essery, R., Boike, J., Langer, M., Heikenfeld, M., Cox, P. and
794 Friedlingstein, P.: An improved representation of physical permafrost dynamics in the JULES
795 land-surface model, *Geosci. Model Dev.*, 8(5), 1493–1508, doi:10.5194/gmd-8-1493-2015,
796 2015.
- 797 Chang, J., Wang, G. X., Li, C. J. and Mao, T. X.: Seasonal dynamics of suprapermafrost
798 groundwater and its response to the freezing-thawing processes of soil in the permafrost
799 region of Qinghai–Tibet Plateau, *Sci. China Earth Sci.*, 58(5), 727–738, doi:10.1007/s11430-
800 014-5009-y, 2015.
- 801 Chen, R., Song, Y., Kang, E., Han, C., Liu, J., Yang, Y., Qing, W. and Liu, Z.: A cryosphere-
802 hydrology observation system in a small alpine watershed in the Qilian mountains of China
803 and its meteorological gradient, *Arctic, Antarct. Alp. Res.*, 46(2), 505–523, doi:10.1657/1938-
804 4246-46.2.505, 2014.
- 805 Chen, R., Wang, G., Yang, Y., Liu, J., Han, C., Song, Y., Liu, Z. and Kang, E.: Effects of
806 Cryospheric Change on Alpine Hydrology: Combining a Model With Observations in the
807 Upper Reaches of the Hei River, China, *J. Geophys. Res. Atmos.*, 123(7), 3414–3442,
808 doi:10.1002/2017JD027876, 2018.
- 809 Chiasson-Poirier, G., Franssen, J., Lafrenière, M. J., Fortier, D. and Lamoureux, S. F.: Seasonal
810 evolution of active layer thaw depth and hillslope-stream connectivity in a permafrost
811 watershed, *Water Resour. Res.*, 56(1), 1–18, doi:10.1029/2019WR025828, 2020.
- 812 Cuo, L., Zhang, Y., Bohn, T. J., Zhao, L., Li, J., Liu, Q. and Zhou, B.: Journal of geophysical
813 research, *Nature*, 175(4449), 238, doi:10.1038/175238c0, 1955.
- 814 Ding, Y., Zhang, S., Chen, R., Han, T., Han, H., Wu, J., Li, X., Zhao, Q., Shangguan, D., Yang, Y.,
815 Liu, J., Wang, S., Qin, J. and Chang, Y.: Hydrological Basis and Discipline System of
816 Cryohydrology: From a Perspective of Cryospheric Science, *Front. Earth Sci.*, 8(December),
817 doi:10.3389/feart.2020.574707, 2020.
- 818 Dobinski, W.: *Permafrost. Earth-Science Reviews*, 108, 158–169, 2011.
- 819 Evans, S. G., Ge, S., Voss, C. I. and Molotch, N. P.: The Role of Frozen Soil in Groundwater
820 Discharge Predictions for Warming Alpine Watersheds, *Water Resour. Res.*, 54(3), 1599–
821 1615, doi:10.1002/2017WR022098, 2018.
- 822 Fabre, C., Sauvage, S., Tananaev, N., Srinivasan, R., Teisserenc, R. and Pérez, J. M. S.: Using
823 modeling tools to better understand permafrost hydrology, *Water (Switzerland)*, 9(6),
824 doi:10.3390/w9060418, 2017.
- 825 Farquharson, L. M., Romanovsky, V. E., Cable, W. L., Walker, D. A., Kokelj, S. V. and Nicolsky,
826 D.: Climate Change Drives Widespread and Rapid Thermokarst Development in Very Cold
827 Permafrost in the Canadian High Arctic, *Geophys. Res. Lett.*, 46(12), 6681–6689,
828 doi:10.1029/2019GL082187, 2019.



- 829 Fenicia, F., Savenije, H. H. G., Matgen, P. and Pfister, L.: Is the groundwater reservoir linear?
830 Learning from data in hydrological modelling, *Hydrol. Earth Syst. Sci.*, 10(1), 139–150,
831 doi:10.5194/hess-10-139-2006, 2006.
- 832 Fenicia, F., Kavetski, D. and Savenije, H. H. G.: Elements of a flexible approach for conceptual
833 hydrological modeling: 1. Motivation and theoretical development, *Water Resour. Res.*,
834 47(11), 1–13, doi:10.1029/2010WR010174, 2011.
- 835 Fenicia, F. and McDonnell, J. J.: Modeling streamflow variability at the regional scale: (1)
836 perceptual model development through signature analysis, *J. Hydrol.*, 605(December 2021),
837 127287, doi:10.1016/j.jhydrol.2021.127287, 2022.
- 838 Gao, B., Yang, D., Qin, Y., Wang, Y., Li, H., Zhang, Y. and Zhang, T.: Change in frozen soils
839 and its effect on regional hydrology, upper Heihe basin, northeastern Qinghai-Tibetan
840 Plateau, *Cryosphere*, 12(2), 657–673, doi:10.5194/tc-12-657-2018, 2018.
- 841 Gao, H., Hrachowitz, M., Fenicia, F., Gharari, S. and Savenije, H. H. G.: Testing the realism of a
842 topography-driven model (FLEX-Topo) in the nested catchments of the Upper Heihe, China,
843 *Hydrol. Earth Syst. Sci.*, 18(5), 1895–1915, doi:10.5194/hess-18-1895-2014, 2014.
- 844 Gao, H.: Landscape-based hydrological modelling: understanding the influence of climate,
845 topography, and vegetation on catchment hydrology, Ph.D. Dissertation, Delft University of
846 Technology, 2015
- 847 Gao, H., Hrachowitz, M., Sriwongsitanon, N., Fenicia, F., Gharar, S.i, and Savenije, H. H. G.:
848 Water Resources Research, *J. Am. Water Resour. Assoc.*, 5(3), 2–2, doi:10.1111/j.1752-
849 1688.1969.tb04897.x, 1969.
- 850 Gao, H., Ding, Y., Zhao, Q., Hrachowitz, M. and Savenije, H. H. G.: The importance of aspect
851 for modelling the hydrological response in a glacier catchment in Central Asia, *Hydrol.*
852 *Process.*, 31(16), 2842–2859, doi:10.1002/hyp.11224, 2017.
- 853 Gao, H., Dong, J., Chen, X., Cai, H., Liu, Z., Jin, Z., Mao, D., Yang, Z. and Duan, Z.: Stepwise
854 modeling and the importance of internal variables validation to test model realism in a data
855 scarce glacier basin, *J. Hydrol.*, 591(September), 125457, doi:10.1016/j.jhydrol.2020.125457,
856 2020.
- 857 Gao, H., Wang, J., Yang, Y., Pan, X., Ding, Y. and Duan, Z.: Permafrost Hydrology of the
858 Qinghai-Tibet Plateau: A Review of Processes and Modeling, *Front. Earth Sci.*, 8(January),
859 doi:10.3389/feart.2020.576838, 2021.
- 860 Gao, J., Xie, Z., Wang, A., Liu, S., Zeng, Y., Liu, B., Li, R., Jia, B., Qin, P. and Xie, J.: A New
861 Frozen Soil Parameterization Including Frost and Thaw Fronts in the Community Land
862 Model, *J. Adv. Model. Earth Syst.*, 11(3), 659–679, doi:10.1029/2018MS001399, 2019.
- 863 Gharari, S., Hrachowitz, M., Fenicia, F., Gao, H. and Savenije, H. H. G.: Using expert
864 knowledge to increase realism in environmental system models can dramatically reduce the
865 need for calibration, *Hydrol. Earth Syst. Sci.*, 18(12), 4839–4859, doi:10.5194/hess-18-4839-
866 2014, 2014.



- 867 Gisnas, K., Westermann, S., Vikhamar Schuler, T., Melvold, K. and Etzelmüller, B.: Small-scale
868 variation of snow in a regional permafrost model, *Cryosphere*, 10(3), 1201–1215,
869 doi:10.5194/tc-10-1201-2016, 2016.
- 870 Gouttevin, I., Krinner, G., Ciais, P., Polcher, J. and Legout, C.: Multi-scale validation of a new
871 soil freezing scheme for a land-surface model with physically-based hydrology, *Cryosphere*,
872 6(2), 407–430, doi:10.5194/tc-6-407-2012, 2012.
- 873 Gupta, H. V., Kling, H., Yilmaz, K. K. and Martinez, G. F.: Decomposition of the mean squared
874 error and NSE performance criteria: Implications for improving hydrological modelling, *J.*
875 *Hydrol.*, 377(1–2), 80–91, doi:10.1016/j.jhydrol.2009.08.003, 2009.
- 876 Han, C., Chen, R., Liu, J., Yang, Y., Liu, Z.: Hydrological characteristics in non-freezing period
877 at the alpine desert zone of Hulugou watershed, Qilian Mountains. *Journal of Glaciology*
878 *and Geocryology*, 35(6), 1536–1544, 2013.
- 879 Han, C., Chen, R., Liu, Z., Yang, Y., Liu, J., Song, Y., Wang, L., Liu, G., Guo, S. and Wang, X.:
880 Cryospheric Hydrometeorology Observation in the Hulu Catchment (CHOICE), Qilian
881 Mountains, China, *Vadose Zo. J.*, 17(1), 180058, doi:10.2136/vzj2018.03.0058, 2018.
- 882 Hülsmann, L., Geyer, T., Schweitzer, C., Priess, J. and Karthe, D.: The effect of subarctic
883 conditions on water resources: initial results and limitations of the SWAT model applied to
884 the Kharaa River Basin in Northern Mongolia, *Environ. Earth Sci.*, 73(2), 581–592,
885 doi:10.1007/s12665-014-3173-1, 2015.
- 886 Immerzeel, W. W., Van Beek, L. P. H. and Bierkens, M. F. P.: Climate change will affect the
887 asian water towers, *Science* (80-.), 328(5984), 1382–1385, doi:10.1126/science.1183188,
888 2010.
- 889 Immerzeel, W. W., Wanders, N., Lutz, A. F., Shea, J. M. and Bierkens, M. F. P.: Reconciling
890 high-altitude precipitation in the upper Indus basin with glacier mass balances and runoff,
891 *Hydrol. Earth Syst. Sci.*, 19(11), 4673–4687, doi:10.5194/hess-19-4673-2015, 2015.
- 892 Jarvis PG.: Prospects for bottom-up models. In *Scaling Physiological Processes: Leaf to*
893 *Globe*. Ehleringer JR, Field CB (eds). Academic Press, 1993.
- 894 Jiang, H., Zheng, G., Yi, Y., Chen, D., Zhang, W., Yang, K. and Miller, C. E.: Progress and
895 Challenges in Studying Regional Permafrost in the Tibetan Plateau Using Satellite Remote
896 Sensing and Models, *Front. Earth Sci.*, 8(December), doi:10.3389/feart.2020.560403, 2020.
- 897 Krogh, S. A., Pomeroy, J. W. and Marsh, P.: Diagnosis of the hydrology of a small Arctic basin
898 at the tundra-taiga transition using a physically based hydrological model, *J. Hydrol.*,
899 550(May), 685–703, doi:10.1016/j.jhydrol.2017.05.042, 2017.
- 900 Kurylyk, B. L., M. Hayashi, W. L. Quinton, J. M. McKenzie, and C. I. Voss: Influence of vertical
901 and lateral heat transfer on permafrost thaw, peatland landscape transition, and
902 groundwater flow, *Water Resour. Res.*, 52, 1286–1305, doi:10.1002/2015WR018057, 2016.
- 903 Lafrenière, M. J., and Lamoureux, S. F.: Effects of changing permafrost conditions on
904 hydrological processes and fluvial fluxes. *Earth-Science Reviews*, 191, 212–223, 2019.



- 905 Li, X., Wu, T., Zhu, X., Jiang, Y., Hu, G., & Hao, J., et al.: Improving the Noah-MP model for
906 simulating hydrothermal regime of the active layer in the permafrost regions of the
907 Qinghai-Tibet Plateau. *Journal of Geophysical Research: Atmospheres*, 125, e2020JD032588.
908 <https://doi.org/10.1029/2020JD032588>, 2020
- 909 Lindstrom, G., Bishop, K., and Lofvenius, M. O.: Soil frost and runoff at Svartberget, northern
910 Sweden—measurements and model analysis. *Hydrol. Process.* 16, 3379–3392, 2002
- 911 Liu, Y., Zhao, L., and Li, R.: Simulation of the soil water-thermal features within the active
912 layer in Tanggula region, Tibetan plateau, by using SHAW model. *J. Glaciol. Geocryol.* 35,
913 280–290, 2013
- 914 Lyon, S. W., Destouni, G., Giesler, R., Humborg, C., Mörth, M., Seibert, J., Karlsson, J. and
915 Troch, P. A.: Estimation of permafrost thawing rates in a sub-arctic catchment using
916 recession flow analysis, *Hydrol. Earth Syst. Sci.*, 13(5), 595–604, doi:10.5194/hess-13-595-
917 2009, 2009.
- 918 Ma, R., Sun, Z., Hu, Y., Chang, Q., Wang, S., Xing, W. and Ge, M.: Hydrological connectivity
919 from glaciers to rivers in the Qinghai-Tibet Plateau: Roles of suprapermafrost and
920 subpermafrost groundwater, *Hydrol. Earth Syst. Sci.*, 21(9), 4803–4823, doi:10.5194/hess-
921 21-4803-2017, 2017.
- 922 Ma, R., Sun, Z., Chang, Q., Ge, M., Pan, Z.: Control of the interactions between stream and
923 groundwater by permafrost and seasonal frost in an alpine catchment, northeastern Tibet
924 Plateau, China. *Journal of Geophysical Research: Atmospheres*, 126, e2020JD033689, 2021
- 925 McNamara, J. P., Kane, D. L. and Hinzman, L. D.: An analysis of streamflow hydrology in the
926 Kuparuk River Basin, Arctic Alaska: A nested watershed approach, *J. Hydrol.*, 206(1–2), 39–
927 57, doi:10.1016/S0022-1694(98)00083-3, 1998.
- 928 Muster, S., Langer, M., Heim, B., Westermann, S. and Boike, J.: Subpixel heterogeneity of ice-
929 wedge polygonal tundra: A multi-scale analysis of land cover and evapotranspiration in the
930 Lena River Delta, Siberia, *Tellus, Ser. B Chem. Phys. Meteorol.*, 64(1), 0–19,
931 doi:10.3402/tellusb.v64i0.17301, 2012.
- 932 Nash, J. and Sutcliffe, J.V.: River Flow Forecasting through Conceptual Models Part I—A
933 Discussion of Principles. *Journal of Hydrology*, 10, 282–290,
934 [http://dx.doi.org/10.1016/0022-1694\(70\)90255-6](http://dx.doi.org/10.1016/0022-1694(70)90255-6), 1970
- 935 Nyberg, L.: Soil frost effects on soil water and runoff dynamics along a boreal forest
936 transect: 1. Field investigations. *Hydrol. Process.* 15, 909–926, 2001.
- 937 Niu, G. Y. and Yang, Z. L.: Effects of frozen soil on snowmelt runoff and soil water storage at
938 a continental scale, *J. Hydrometeorol.*, 7(5), 937–952, doi:10.1175/JHM538.1, 2006.
- 939 Niu L, Ye B S, Li J, et al.: Effect of permafrost degradation on hydrological processes in
940 typical basins with various permafrost coverage in Western China. *Sci China Earth Sci*, doi:
941 10.1007/s11430-010-4073-1, 2010.
- 942 Nitze, I., Grosse, G., Jones, B. M., Romanovsky, V. E. and Boike, J.: Remote sensing quantifies



- 943 widespread abundance of permafrost region disturbances across the Arctic and Subarctic,
944 Nat. Commun., 9(1), 1–11, doi:10.1038/s41467-018-07663-3, 2018.
- 945 Oleson, K. and Lawrence, D.: NCAR / TN-503 + STR NCAR Technical Note July 2013
946 Technical Description of version 4 . 5 of the Community Land Model (CLM), (March 2014),
947 2013.
- 948 Osuch, M., Wawrzyniak, T. and Nawrot, A.: Diagnosis of the hydrology of a small Arctic
949 permafrost catchment using HBV conceptual rainfall-runoff model, Hydrol. Res., 50(2), 459–
950 478, doi:10.2166/nh.2019.031, 2019.
- 951 Pan, X., Li, Y., Yu, Q., Shi, X., Yang, D. and Roth, K.: Effects of stratified active layers on high-
952 altitude permafrost warming: A case study on the Qinghai-Tibet Plateau, Cryosphere, 10(4),
953 1591–1603, doi:10.5194/tc-10-1591-2016, 2016.
- 954 Pan, X., Yu, Q., You, Y., Chun, K. P., Shi, X. and Li, Y.: Contribution of supra-permafrost
955 discharge to thermokarst lake water balances on the northeastern Qinghai-Tibet Plateau, J.
956 Hydrol., 555(November), 621–630, doi:10.1016/j.jhydrol.2017.10.046, 2017.
- 957 Pan, Z., Sun, Z., Hu, Y., Chang, Q., Ge, M., Wang, S., Bu, J., Long, X., Pan, Y. and Zhao, L.:
958 Datasets for research on groundwater flow and its interactions with surface water in an
959 alpine catchment on the northeastern Tibetan Plateau, China, , (September), 2021.
- 960 Pianosi, F. and Wagener, T.: Understanding the time-varying importance of different
961 uncertainty sources in hydrological modelling using global sensitivity analysis, Hydrol.
962 Process., 30(22), 3991–4003, doi:10.1002/hyp.10968, 2016.
- 963 Ran, Y., Li, X., Cheng, G., Nan, Z., Che, J., Sheng, Y., Wu, Q., Jin, H., Luo, D., Tang, Z. and Wu,
964 X.: Mapping the permafrost stability on the Tibetan Plateau for 2005–2015, Sci. China Earth
965 Sci., 64(1), 62–79, doi:10.1007/s11430-020-9685-3, 2021.
- 966 Savenije, H.H.G.:HESS Opinions: “The art of hydrology”. Hydrol. Earth Syst. Sci., 13, 157–161,
967 2009
- 968 Savenije, H.H.G.: HESS Opinions “Topography driven conceptual modelling (FLEXTopo)”.
969 Hydrol. Earth Syst. Sci. 14 (12), 2681–2692. <https://doi.org/10.5194/hess-14-2681-2010>,
970 2010.
- 971 Seibert, J. and McDonnell, J. J.: On the dialog between experimentalist and modeler in
972 catchment hydrology: Use of soft data for multicriteria model calibration, Water Resour.
973 Res., 38(11), 23-1-23–14, doi:10.1029/2001wr000978, 2002.
- 974 Shanley, J. B. and Chalmers, A.: The effect of frozen soil on snowmelt runoff at Sleepers
975 River, Vermont, Hydrol. Process., 13(12–13), 1843–1857, doi:10.1002/(SICI)1099-
976 1085(199909)13:12/13<1843::AID-HYP879>3.0.CO;2-G, 1999.
- 977 Sheng, Y.: Map of permafrost distribution in the Qilian Mountains. National Tibetan Plateau
978 Data Center, doi:10.11888/Geocry.tpd.270456. CSTR: 18406.11.Geocry.tpd.270456, 2020.
- 979 Sivapalan, M., Blöschl, G., Zhang, L. and Vertessy, R.: Downward approach to hydrological
980 prediction, Hydrol. Process., 17(11), 2101–2111, doi:10.1002/hyp.1425, 2003.



- 981 Sjöberg, Y., Frampton, A. and Lyon, S. W.: Using streamflow characteristics to explore
982 permafrost thawing in northern Swedish catchments, *Hydrogeol. J.*, 21(1), 121–131,
983 doi:10.1007/s10040-012-0932-5, 2013.
- 984 Sokolov, K., Fedorova, L. and Fedorov, M.: Prospecting and evaluation of underground
985 massive ice by ground-penetrating radar, *Geosci.*, 10(7), 1–14,
986 doi:10.3390/geosciences10070274, 2020.
- 987 Streletskiy, D. A., Tananaev, N. I., Opel, T., Shiklomanov, N. I., Nyland, K. E., Streletskaya, I. D.,
988 Tokarev, I. and Shiklomanov, A. I.: Permafrost hydrology in changing climatic conditions:
989 Seasonal variability of stable isotope composition in rivers in discontinuous permafrost,
990 *Environ. Res. Lett.*, 10(9), doi:10.1088/1748-9326/10/9/095003, 2015.
- 991 Sun, A., Quantified hydrological responses to permafrost degradation in the headwaters of
992 the Yellow River (HWYR) in High Asia. *Science of the Total Environment*, 712135632
993 Permafrost Hydrology Research Domain: Process-Based Adjustment, 2020.
- 994 Sun, Z., Zhao, L., Hu, G., Qiao, Y., Du, E., Zou, D., et al: Modeling permafrost changes on the
995 Qinghai-Tibetan plateau from 1966 to 2100: a case study from two boreholes along the
996 Qinghai-Tibet engineering corridor. *Permafr. Periglac. Process.* 31, 156–171,
997 doi:10.1002/ppp.2022, 2019.
- 998 Tananaev, N., Teisserenc, R. and Debolskiy, M.: Permafrost hydrology research domain:
999 Process-based adjustment, *Hydrology*, 7(1), doi:10.3390/hydrology7010006, 2020.
- 1000 Walvoord, M. A. and Kurylyk, B. L.: Hydrologic Impacts of Thawing Permafrost-A Review,
1001 *Vadose Zo. J.*, 15(6), vzi2016.01.0010, doi:10.2136/vzi2016.01.0010, 2016.
- 1002 Wang, G. X., Mao, T. X., Chang, J., Song, C. L., and Huang, K. W.: Processes of runoff
1003 generation operating during the spring and autumn seasons in a permafrost catchment on
1004 semi-arid plateaus. *J. Hydrol.* 550, 307–317. doi:10.1016/j.jhydrol.2017.05.020, 2017.
- 1005 Wang, L., Koike, T., Yang, K., Jin, R. and Li, H.: Frozen soil parameterization in a distributed
1006 biosphere hydrological model, *Hydrol. Earth Syst. Sci.*, 14(3), 557–571, doi:10.5194/hess-14-
1007 557-2010, 2010.
- 1008 Wang, P., Huang, Q., Pozdniakov, S. P., Liu, S., Ma, N., Wang, T., Zhang, Y., Yu, J., Xie, J., Fu,
1009 G., Frolova, N. L. and Liu, C.: Potential role of permafrost thaw on increasing Siberian river
1010 discharge, *Environ. Res. Lett.*, 16(3), doi:10.1088/1748-9326/abe326, 2021.
- 1011 Wang Q F, Jin H J, Zhang T J, et al.: Active layer seasonal freeze-thaw processes and
1012 influencing factors in the alpine permafrost regions in the upper reaches of the Heihe River
1013 in Qilian Mountains (in Chinese). *Chin Sci Bull*, 61: 2742–2756, doi: 10.1360/N972015-01237,
1014 2016.
- 1015 Wang, T., Yang, D., Yang, Y., Piao, S., Li, X., Cheng, G. and Fu, B.: Permafrost thawing puts
1016 the frozen carbon at risk over the Tibetan Plateau, *Sci. Adv.*, 6(19), 2–10,
1017 doi:10.1126/sciadv.aaz3513, 2020.
- 1018 Wang, Y., Yang, H., Gao, B., Wang, T., Qin, Y. and Yang, D.: State Key Laboratory of



- 1019 Hydrosience and Engineering , Department of Hydraulic School of Water Resources and
1020 Environment , China University of Geosciences , 2018.
- 1021 Watson, V., Kooi, H. and Bense, V.: Potential controls on cold-season river flow behavior in
1022 subarctic river basins of Siberia, *J. Hydrol.*, 489, 214–226, doi:10.1016/j.jhydrol.2013.03.011,
1023 2013.
- 1024 Woo, M-K.: *Permafrost Hydrology*, Springer, 5, 2012.
- 1025 Wu, T., Li, S., Cheng, G. and Nan, Z.: Using ground-penetrating radar to detect permafrost
1026 degradation in the northern limit of permafrost on the Tibetan Plateau, *Cold Reg. Sci.*
1027 *Technol.*, 41(3), 211–219, doi:10.1016/j.coldregions.2004.10.006, 2005.
- 1028 Xiao, Y., Zhao, L., Dai, Y., Li, R., Pang, Q. and Yao, J.: Representing permafrost properties in
1029 CoLM for the Qinghai-Xizang (Tibetan) Plateau, *Cold Reg. Sci. Technol.*, 87, 68–77,
1030 doi:10.1016/j.coldregions.2012.12.004, 2013.
- 1031 Xie, C., Gough, W.A.: Short Communication: A Simple Thaw-Freezing Algorithm for a Multi-
1032 Layered Soil using the Stefan Equation. *Permafrost and Periglac. Process.* 24: 252–260, 2013.
- 1033 Yang, Y., Wu, Q., Jin, H., Wang, Q., Huang, Y., Luo, D., Gao, S. and Jin, X.: Delineating the
1034 hydrological processes and hydraulic connectivities under permafrost degradation on
1035 Northeastern Qinghai-Tibet Plateau, China, *J. Hydrol.*, 569(November 2018), 359–372,
1036 doi:10.1016/j.jhydrol.2018.11.068, 2019.
- 1037 Ye, B., Yang, D., Zhang, Z. and Kane, D. L.: Variation of hydrological regime with permafrost
1038 coverage over Lena Basin in Siberia, *J. Geophys. Res. Atmos.*, 114(7),
1039 doi:10.1029/2008JD010537, 2009.
- 1040 Zhang, R., Liu, J., Gao, H. and Mao, G.: Can multi-objective calibration of streamflow
1041 guarantee better hydrological model accuracy?, *J. Hydroinformatics*, 20(3), 687–698,
1042 doi:10.2166/hydro.2018.131, 2018.
- 1043 Zhang, T., Frauenfeld, O. W., Serreze, M. C., Etringer, A., Oelke, C., McCreight, J., Barry, R. G.,
1044 Gilichinsky, D., Yang, D., Ye, H., Ling, F. and Chudinova, S.: Spatial and temporal variability in
1045 active layer thickness over the Russian Arctic drainage basin, *J. Geophys. Res. D Atmos.*,
1046 110(16), 1–14, doi:10.1029/2004JD005642, 2005.
- 1047 Zhang, X. : High-resolution precipitation data derived from dynamical downscaling using
1048 the WRF model for the Heihe River Basin, northwest China. *Theor Appl Climatol*, 131:1249–
1049 1259, 2018.
- 1050 Zhao, L., Zou, D., Hu, G., Du, E., Pang, Q., Xiao, Y., Li, R., Sheng, Y., Wu, X., Sun, Z., Wang, L.,
1051 Wang, C., Ma, L., Zhou, H. and Liu, S.: Changing climate and the permafrost environment on
1052 the Qinghai–Tibet (Xizang) plateau, *Permafr. Periglac. Process.*, 31(3), 396–405,
1053 doi:10.1002/ppp.2056, 2020.
- 1054 Zhou, J., Kinzelbach, W., Cheng, G., Zhang, W., He, X. and Ye, B.: Monitoring and modeling
1055 the influence of snow pack and organic soil on a permafrost active layer, qinghai-tibetan
1056 plateau of china, *Cold Reg. Sci. Technol.*, 90–91, 38–52,



1057 doi:10.1016/j.coldregions.2013.03.003, 2013.
 1058 Zou, D., Zhao, L., Wu, T., Wu, X., Pang, Q. and Wang, Z.: Modeling ground surface
 1059 temperature by means of remote sensing data in high-altitude areas: test in the central
 1060 Tibetan Plateau with application of moderate-resolution imaging spectroradiometer
 1061 Terra/Aqua land surface temperature and ground-based infrared, J. Appl. Remote Sens.,
 1062 8(1), 083516, doi:10.1117/1.jrs.8.083516, 2014.
 1063

1064 Tables

1065 Table 1. The water balance and constitutive equations used in FLEX-Topo-FS model. In Equation
 1066 10, 11, and 12, the S_u and $S_{u\max}$ represent root zone reservoirs and their storage capacities in
 1067 different landscapes, including vegetation hillslope ($S_{u\max,V}$), alpine desert ($S_{u\max,D}$) and riparian
 1068 ($S_{u\max,R}$).

reservoirs	Water balance equations	Constitutive equations
Snow reservoir	$\frac{dS_w}{dt} = P - M_w \quad (4)$	$P_s = \begin{cases} 0; & T > 0 \\ P; & T \leq 0 \end{cases} \quad (5)$
		$M_w = \begin{cases} F_{dd} \cdot T; & T > 0 \\ 0; & T \leq 0 \end{cases} \quad (6)$
Glacier reservoir	$\frac{dS_g}{dt} = P_l + M_g - Q_g \quad (7)$	$M_g = \begin{cases} F_{dd} \cdot T \cdot C_g; & S_w = 0 \text{ and } T > 0 \\ 0; & S_w > 0 \text{ or } T \leq 0 \end{cases} \quad (8)$
		$Q_g = S_g / K_f \quad (9)$
Root zone reservoir	$\frac{dS_u}{dt} = P_l + M_w - E_a - R_u \quad (10)$	$R_u = (P_l + M_w) \cdot \left(1 - \left(1 - \frac{S_u}{S_{u\max}}\right)^\beta\right) \quad (11)$
		$E_a = E_p \cdot \left(\frac{S_u}{C_e \cdot S_{u\max}}\right) \quad (12)$
Splitter and lag function		$R_f = R_u D \quad (13); \quad R_s = R_u (1 - D) \quad (14)$
		$R_{fl}(t) = \sum_{i=1}^{T_{lag}} c_f(i) \cdot R_f(t - i + 1) \quad (15)$



$$c_f(i) = i / \sum_{u=1}^{T_{lagf}} u \quad (16)$$

Fast reservoir $\frac{dS_f}{dt} = R_f - Q_f \quad (17)$ $Q_f = S_f / K_f \quad (18)$

1069

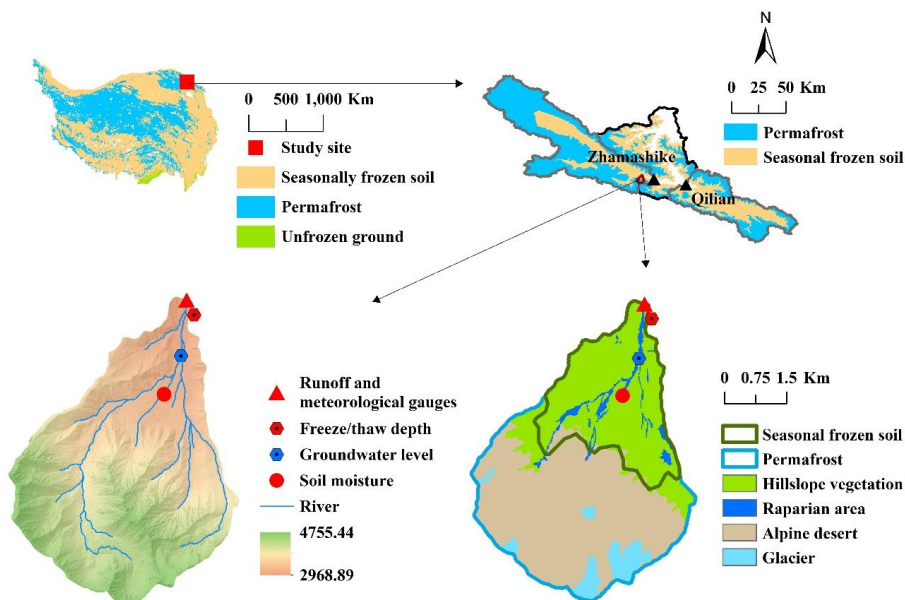
1070 Table 2. The parameters of the FLEX-Topo-FS model, and their prior ranges for calibration.

Parameter	Explanation	Prior range for calibration
$F_{dd}(\text{mm} \cdot \text{°C}^{-1} \cdot \text{d}^{-1})$	snow degree-day factor	(1-5)
$C_g(-)$	Glacier degree-factor multiplier	(1-3)
$S_{\text{max},v}(\text{mm})$	Root zone storage capacity for vegetation hillslope	(50, 200)
$S_{\text{max},d}(\text{mm})$	Root zone storage capacity for alpine desert	(10, 100)
$S_{\text{max},r}(\text{mm})$	Root zone storage capacity for riparian	(10, 100)
$\beta(-)$	The shape of the storage capacity curve	(0, 1)
$C_e(-)$	Soil moisture threshold for reduction of evaporation	(0.1, 1)
$D(-)$	Splitter to fast and slow response reservoirs	0.2
$T_{lagf}(\text{days})$	Lag time from rainfall to peak flow	(0.8, 3)
$K_f(\text{days})$	fast recession coefficient	(1, 10)
$K_s(\text{days})$	baseflow recession coefficient	(10, 100)
$k(W/(m \cdot K))$	thermal conductivity	2
$\omega(-)$	water content, as a decimal fraction of the dry soil weight	0.12
$\rho(\text{kg/m}^3)$	bulk density of the soil	1000

1071



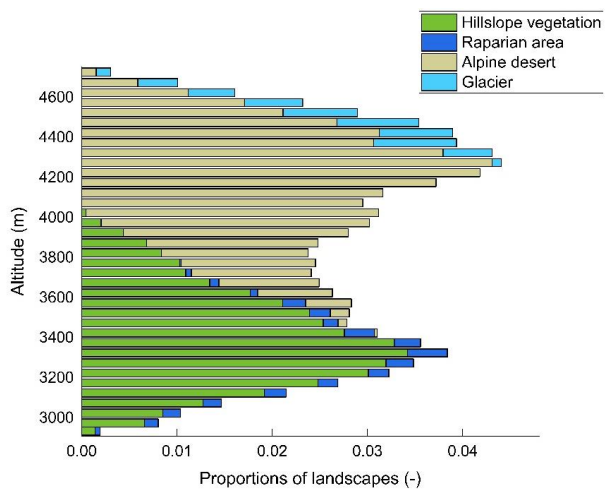
1072 **Figures**



1073

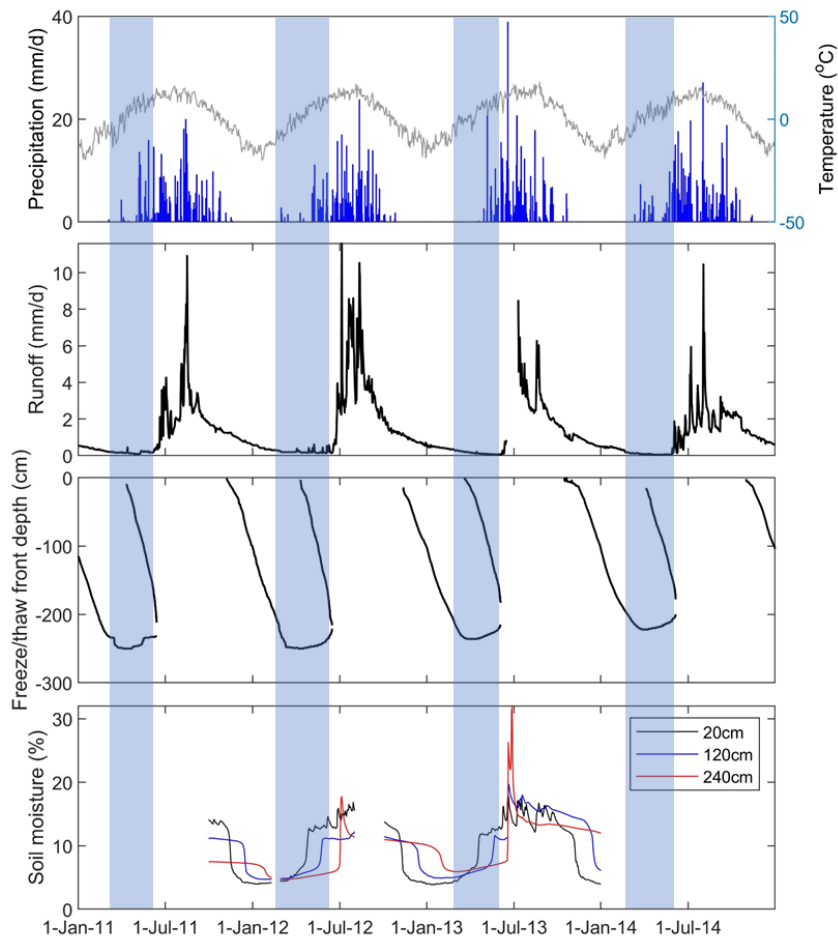
1074 Figure 1. Sketch map of the Tibetan Plateau, and the distribution of permafrost and
1075 seasonal frozen-soil of the Tibetan Plateau (Zou et al., 2014), and the location of the upper
1076 Heihe River basin (up left); sketch map of permafrost and seasonal frozen-soil distribution
1077 of the upper Heihe river basin (Sheng, 2020), and the two sub-basins, i.e. Zhamashike and
1078 Qilian, and the location of the Hulu catchment (up right); Hulu catchment's digital elevation
1079 model (DEM), river channel, runoff and meteorological gauge station, the locations for soil
1080 moisture, groundwater level, and freeze/thaw depth (bottom left); landscapes and seasonal
1081 frozen-soil / permafrost map of the Hulu catchment (bottom right).

1082



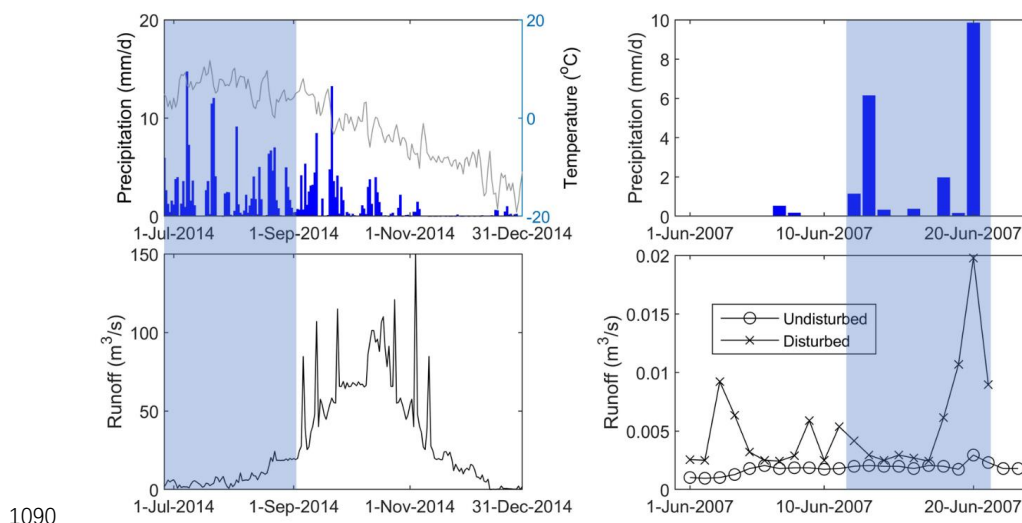
1083

1084 Figure 2. Landscape classification at different elevation bands (with 50m interval) of the Hulu
1085 catchment.



1086

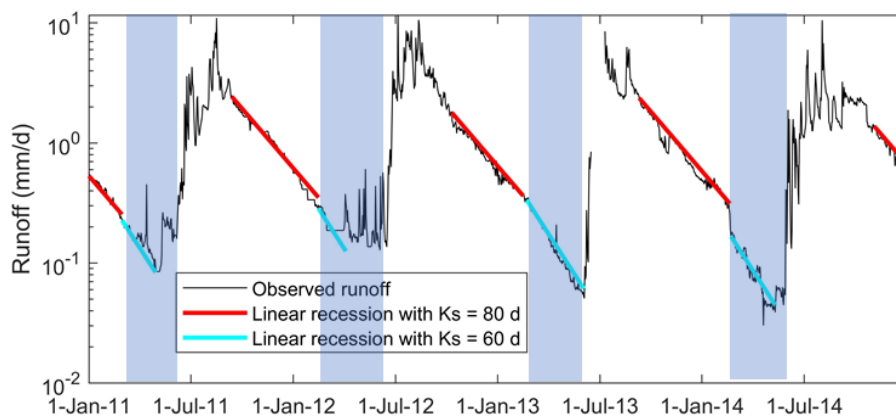
1087 Fig 3. Observed daily precipitation and air temperature; observed daily runoff depth of the
1088 Hulu catchment; observed freeze/thaw front depth; observed soil moisture at the depth of
1089 20cm, 120cm, 240cm.



1090

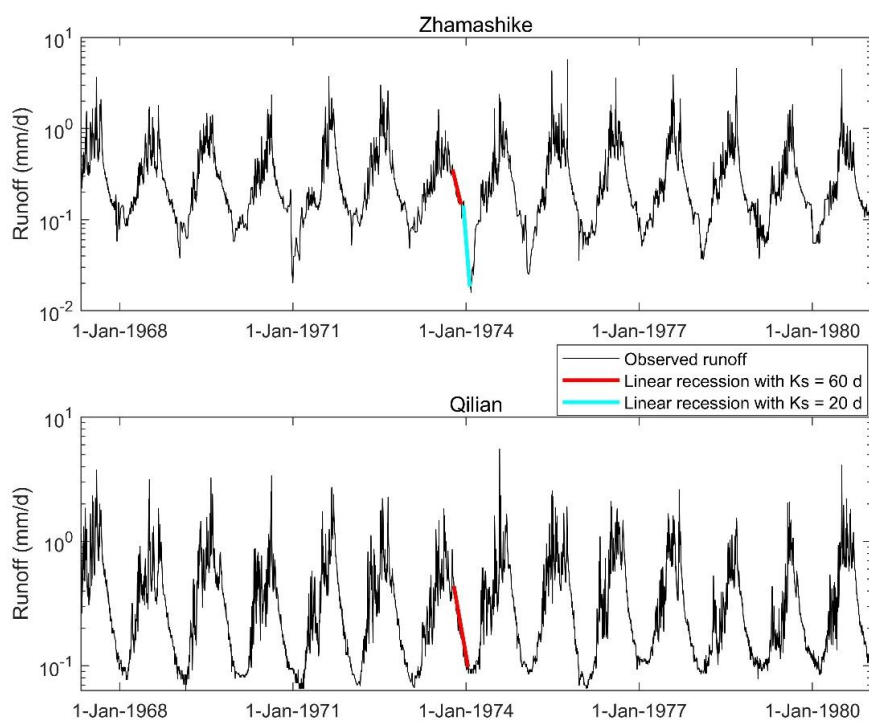
1091 Fig 4. The Little-Runoff in the Early Thawing season (LRET) phenomenon in other places, e.g.
 1092 the headwater of Yellow River (Yang et al., 2019), and the Cape Bounty Arctic Watershed
 1093 Observatory, Melville Island, NU in Canada (Lafrenière and Lamoureux, 2019)

1094



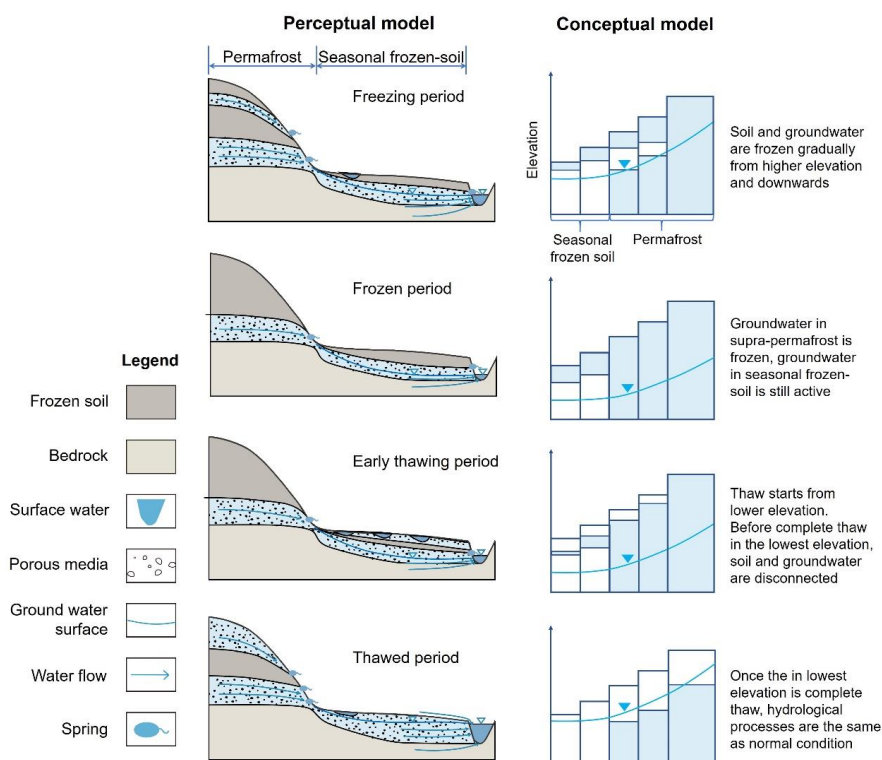
1095

1096 Figure 5. Groundwater recession, from 2011 to 2014, on logarithmic scale, with linear
 1097 recession parameter $K_s = 80$ d in the early recession periods and $K_s = 60$ d in the end of
 1098 recession periods.



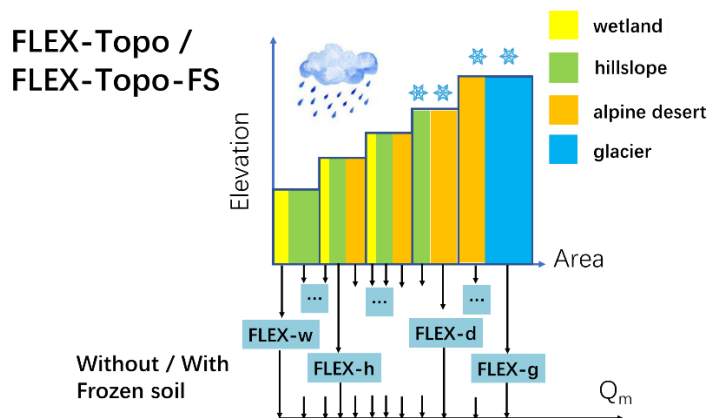
1099

1100 Figure 6. The hydrograph of the Zhamashike and Qilian sub-basin on logarithmic scale, and
1101 the linear recession curve with $K_s = 60$ d and $K_s = 20$ d.



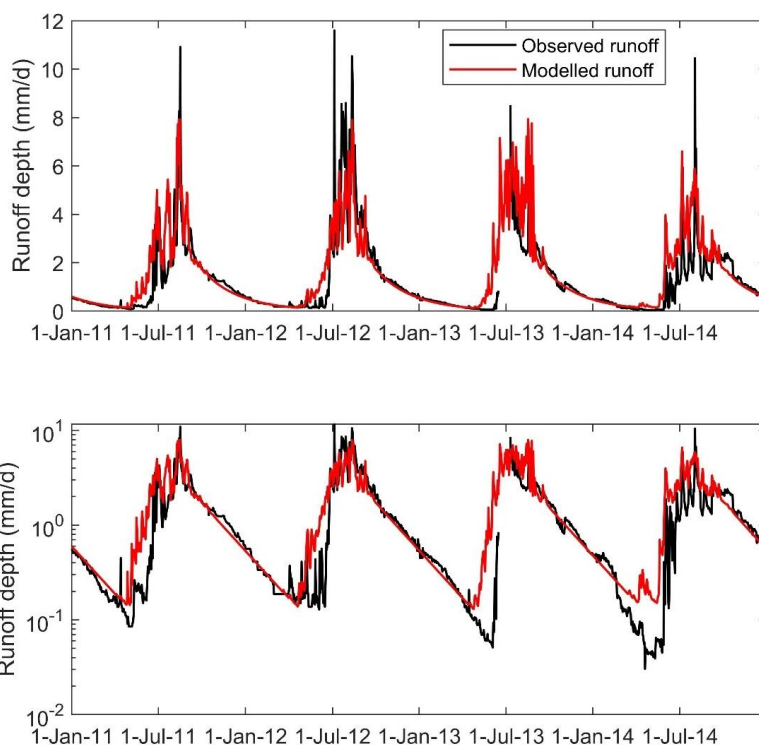
1102

1103 Figure 7 The perceptual and conceptual FLEX-Topo-FS frozen-soil hydrological models.



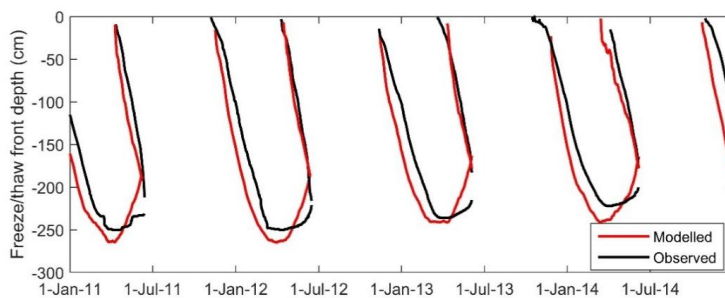
1104

1105 Fig 8. Model structures of FLEX-Topo, and FLEX-Topo-FS



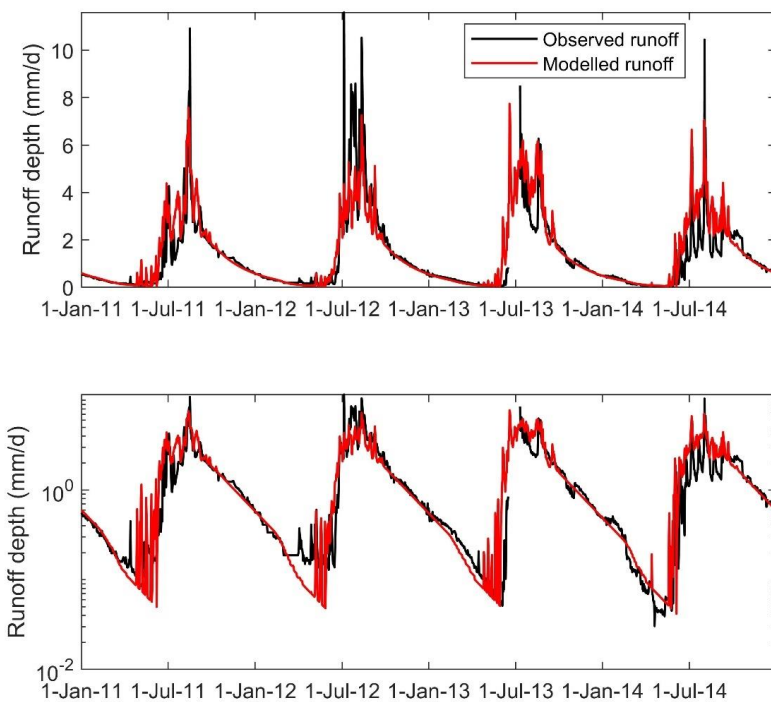
1106

1107 Figure 9. Modeling results of FLEX-Topo, and the comparisons with observation, on both
1108 normal and logarithm scales.



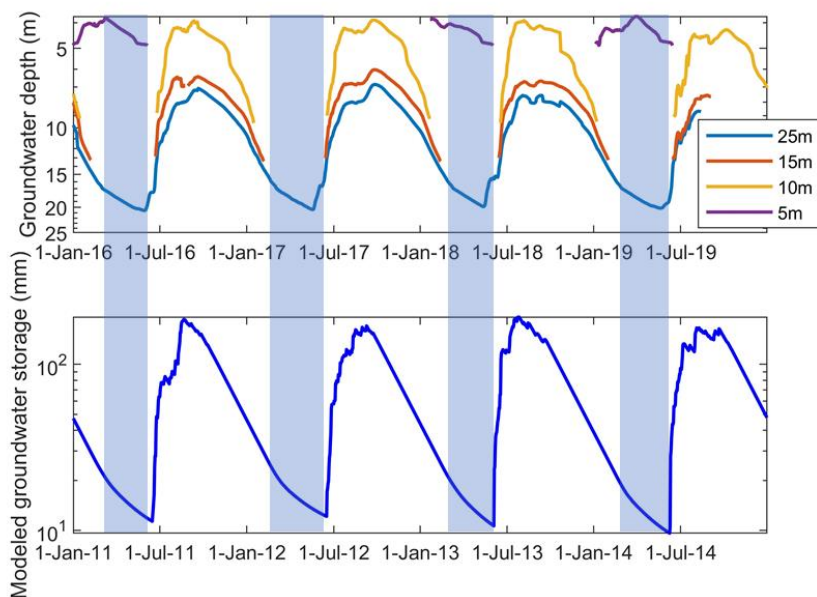
1109

1110 Fig 10. Comparison between simulated freeze/thaw depth by Stefan equation and
1111 observation.



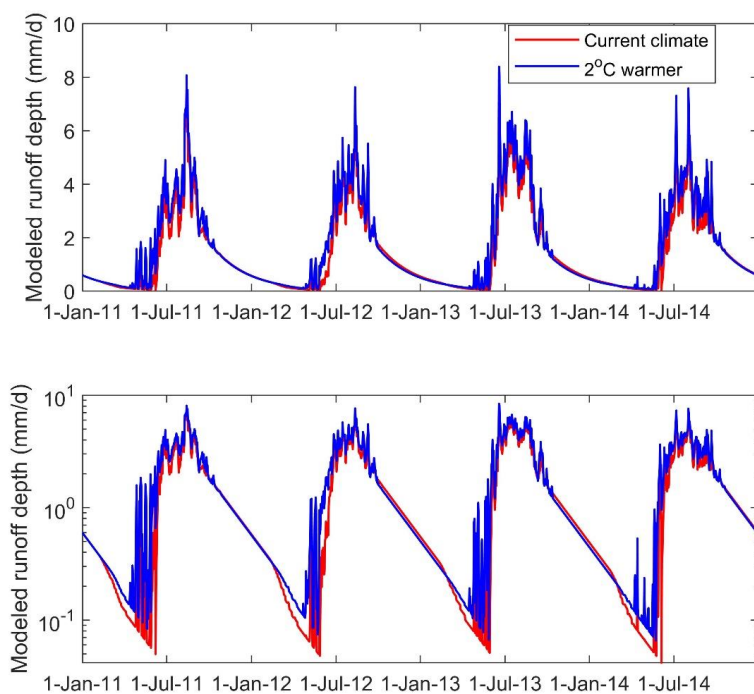
1112

1113 Figure 11. Modeling results of FLEX-Topo-FS, and the comparisons with observation, on
1114 both normal and logarithm scales.



1115

1116 Figure 12. Observed groundwater depth from 2016 to 2019 at WW01 wells at depth of 5m,
1117 10m, 15m, and 25m. And the simulated groundwater storage by the FLEX-Topo-FS model
1118 from 2011 to 2014.



1119

1120 Figure 13. Simulated hydrograph in current climate condition, and the 2°C warmer
1121 condition.